AJS American Journal of Science
publishing earth-sciences research since 1818

Busch, J. F., Boag, T. H., Sperling, E. A., Rooney, A. D., Feng, X., Moynihan, D. P., & Strauss, J. V. (2023). Integrated Litho-, Chemo- and Sequence Stratigraphy of the Ediacaran Gametrail Formation Across a Shelf-Slope Transect in the Wernecke Mountains, Yukon, Canada. *American Journal of Science*, *323*, 4. https://doi.org/10.2475/001c.74874

Science Paper

Integrated Litho-, Chemo- and Sequence Stratigraphy of the Ediacaran Gametrail Formation Across a Shelf-Slope Transect in the Wernecke Mountains, Yukon, Canada

James F. Busch[1], Thomas H. Boag[2,3], Erik A. Sperling[2], Alan D. Rooney[3], Xiahong Feng[1], David P. Moynihan[4], Justin V. Strauss[1a]

[1] Department of Earth Sciences, Dartmouth College, [2] Department of Geological Sciences, Stanford University, [3] Department of Earth and Planetary Sciences, Yale University, [4] Yukon Geological Survey

Keywords: Gametrail Formation, Windermere Supergroup, Ediacaran, Shuram carbon isotope excursion, chemostratigraphy

https://doi.org/10.2475/001c.74874

American Journal of Science

Vol. 323, 2023

The Ediacaran Gametrail Formation of northwestern Canada chronicles the evolution of a complex carbonate ramp system in response to fluctuations in relative sea level and regional tectonic subsidence alongside exceptional global change associated with the Shuram carbon isotope excursion (CIE). Here, we use extensive outcrop exposures of the Gametrail Formation in the Wernecke Mountains of Yukon, Canada, to construct a shelf-slope transect across the Shuram CIE. Twelve stratigraphic sections of the Gametrail Formation are combined with geological mapping and a suite of geochemical analyses to develop an integrated litho-, chemo-, and sequence stratigraphic model for these strata. In the more proximal Corn/Goz Creek region, the Gametrail Formation represents a storm-dominated inner to outer ramp depositional setting, while slope depositional environments in the Nadaleen River region are dominated by hemipelagic sedimentation, turbidites, and debris flows. The magnitude of the Shuram CIE is largest in slope limestones which underwent sediment-buffered diagenesis, while the CIE is notably smaller in the inner-outer ramp dolostones which experienced fluid-buffered diagenesis. Our regional mapping identified a distinct structural panel within the shelf-slope transect that was transported ~30 km via strike-slip motion during the Mesozoic–Cenozoic Cordilleran orogeny. One location in this transported structural block contains a stromatolite reef complex with extremely negative carbon isotope values down to ~ -30‰, while the other location contains an overthickened ooid shoal complex that does not preserve the characteristic negative CIE associated with the Shuram event. These deviations from the usual expression of the Shuram CIE along the shelf-slope transect in the Wernecke Mountains, and elsewhere globally, provide useful examples for how local tectonic, stratigraphic, and/or geochemical complexities can result in unusually large or completely absent expressions of a globally recognized CIE.

1. Introduction

Neoproterozoic carbonate rocks are a primary record of the profound biological and climatic changes which occurred in the prelude to the Cambrian explosion. This is because carbonate rocks commonly encode sedimentological, biological, and primary geochemical information from seawater at the time of their deposition. Northwestern Canada (Yukon and Northwest Territories, NWT) hosts extensive exposures of Neoproterozoic carbonate successions, many of which form an integral part of global paleontological and geochemical compilations from this time interval (for example, Halverson et al., 2005; Kaufman et al., 1997; Macdonald et al., 2010, 2013; Rooney et al., 2015). The carbonate carbon ($\delta^{13}C$) record of Neoproterozoic carbonate rocks is unique in the geological record for its volatility, which is thought to have resulted from a more unstable global carbon cycle prior to the advent of biomineralization and the expansion of the neritic carbonate factory in the Paleozoic (for example, Zeebe & Westbroek, 2003).

The late Neoproterozoic *ca.* 575–567 Ma Shuram carbon isotope excursion (CIE) is the largest known carbonate car-

a Corresponding author:
justin.v.strauss@dartmouth.edu

bon isotope perturbation in Earth history and occurs just after the *ca.* 580 Ma regional Gaskiers glaciation and the first appearance of the Ediacaran Avalon fossil assemblage (Canfield et al., 2020; Grotzinger et al., 2011; Matthews et al., 2021; Rooney et al., 2020). The Shuram CIE has been previously documented in the Gametrail and Last Chance formations of the Mackenzie, Wernecke, and Ogilvie Mountains of central Yukon and western NWT (Busch et al., 2021; Macdonald et al., 2013; Moynihan et al., 2019; Pyle et al., 2004). The exceptional exposure and preservation of the Gametrail Formation (Fm) in this region makes it an important resource for understanding the geological and paleoceanographic origin of the Shuram CIE (Busch et al., 2022). Furthermore, the Gametrail Fm's clear stratigraphic position directly above the first appearance of Ediacaran fossils in northwestern Canada provides a unique opportunity to investigate the environmental context surrounding the proliferation of the first putative metazoan fossil assemblages (Moynihan et al., 2019; Sperling et al., 2015). In addition, preliminary studies of the Gametrail Fm's extensive outcrop distribution in the Wernecke Mountains indicates that it encompasses both proximal and distal environments (Aitken, 1989; Fritz et al., 1983; Macdonald et al., 2013; Pyle et al., 2004); thus, this region serves as an important archive of the Shuram CIE's expression across a paleobathymetric transect.

A multitude of models have been proposed for the origin of the Shuram CIE, including disconnection from open ocean DIC, diagenetic alteration in both deep and shallow burial environments, methane release, authigenic carbonate formation, and non-steady state carbon cycle behavior primarily involving the oxidation of a large pool of isotopically negative dissolved organic carbon (DOC) (for example, Bjerrum & Canfield, 2011; Derry, 2010; Fike et al., 2006; Knauth & Kennedy, 2009; Li et al., 2017; Rothman et al., 2003; Schrag et al., 2013). The role of carbonate diagenesis in driving the Shuram CIE and other large CIEs in the Neoproterozoic continues to be debated as the origin of the anomaly eludes a definitive explanation (Ahm et al., 2021; Burns & Matter, 1993; Cui et al., 2017; Derry, 2010; Knauth & Kennedy, 2009). Busch et al. (2022) recently investigated the role of diagenesis in the expression of the Shuram CIE with a global geochemical and stratigraphic compilation and suggested that burial and meteoric diagenesis were not driving mechanisms for the excursion; instead, changes to the locus and intensity of primary productivity in shallow marine environments may have facilitated local isotope reservoir effects that drove the Shuram CIE. To provide more sedimentological, geochemical, and stratigraphic context for the Shuram CIE in northwestern Canada, we constructed a shelf-slope transect of the Gametrail Fm in the Wernecke Mountains. By combining the sedimentology and sequence stratigraphy of this unit along a paleobathymetric transect with geochronological measurements (Re-Os) and a suite of geochemical analyses (that is, $\delta^{44/40}$Ca, Sr/Ca, Mn/Sr, U/Ca) used for deconvolving the effects of mineralogy and early marine diagenesis on paleoenvironmental proxies, we aim to provide new insights on the global expression of this enigmatic geochemical event.

1.1. Geological Background and Previous Work

Proterozoic strata of the Wernecke Mountains are exposed along the southeastern apex of the Yukon block, a triangular-shaped region in north-central Yukon that formed a relatively high-standing crustal block throughout much of the early Paleozoic (fig. 1; Jeletzky, 1962; Morrow, 1999). The Wernecke Mountains contain exposures of the *ca.* 1.7–1.4 Ga Wernecke Supergroup, the *ca.* 1.2–0.78 Ga Mackenzie Mountains Supergroup, and the *ca.* 0.78–0.54 Ga Windermere Supergroup (fig. 1; Eisbacher, 1981; Macdonald et al., 2013, 2018; Medig et al., 2016; Pyle et al., 2004; Strauss et al., 2015; Thorkelson et al., 2005; Young et al., 1979). The Neoproterozoic Windermere Supergroup contains three km-scale shale to carbonate "Grand Cycles" (Aitken, 1966, 1978, 1989) that likely represent first-order depositional sequences within what has been interpreted as a simple passive margin succession (Mustard, 1991; Mustard & Roots, 1997; Narbonne & Aitken, 1995; Ross, 1991; Ross et al., 1995).

Recent studies have highlighted evidence for protracted Neoproterozoic-early Paleozoic extensional tectonism and sedimentation throughout northwestern Canada (for example, Beranek, 2017; Busch et al., 2021; Campbell et al., 2019; Maurice Colpron et al., 2002; Link et al., 2017; Moynihan et al., 2019; Post & Long, 2008; Strauss et al., 2015). Additionally, paleomagnetic data from the Mount Harper volcanic rocks of the Coal Creek inlier suggest the Yukon block may have been rotated counterclockwise relative to autochthonous Laurentia in the Cryogenian–Ediacaran (Eyster et al., 2016). Collectively, these different lines of evidence suggest that a simple passive continental margin was not established until well after deposition of the Windermere Supergroup, most likely not until the middle to late Cambrian (Moynihan et al., 2019, and references therein).

Ediacaran strata of the uppermost Windermere Supergroup in the Wernecke Mountains have been assigned to the Rackla Group (Moynihan et al., 2019) and include six separate units (fig. 2): an ~100-350 m thick fine-grained siliciclastic succession called the Sheepbed Fm (Gabrielse et al., 1973), an ~60-750 m thick mixed siliciclastic-carbonate unit called the Nadaleen Fm (Moynihan et al., 2019), the ~80-650 m thick carbonate Gametrail Fm that is described herein (Aitken, 1989), an ~100-550 m thick mixed siliciclastic-carbonate succession called the Blueflower Fm (Aitken, 1989), and an ~50-100 m thick carbonate unit called the Risky Fm, which is correlative with an ~100-300 m thick carbonate unit called the Algae Fm in the southern Wernecke Mountains (formerly of the Hyland Group; Cecile, 2000; Moynihan et al., 2019). The base of the Sheepbed Fm was dated to *ca.* 632 Ma (Rooney et al., 2015), while the upper Nadaleen Fm has been dated to *ca.* 575 Ma (Rooney et al., 2020). The Gametrail Fm has no previous geochronological constraints, but a new Re-Os date from the second depositional sequence of the unit is presented herein (*see below*). The Fireweed member of the Last Chance Fm, which is correlative with the upper Gametrail Fm (fig. 2; Busch et al., 2021), has been dated to *ca.* 567 Ma in the adjacent

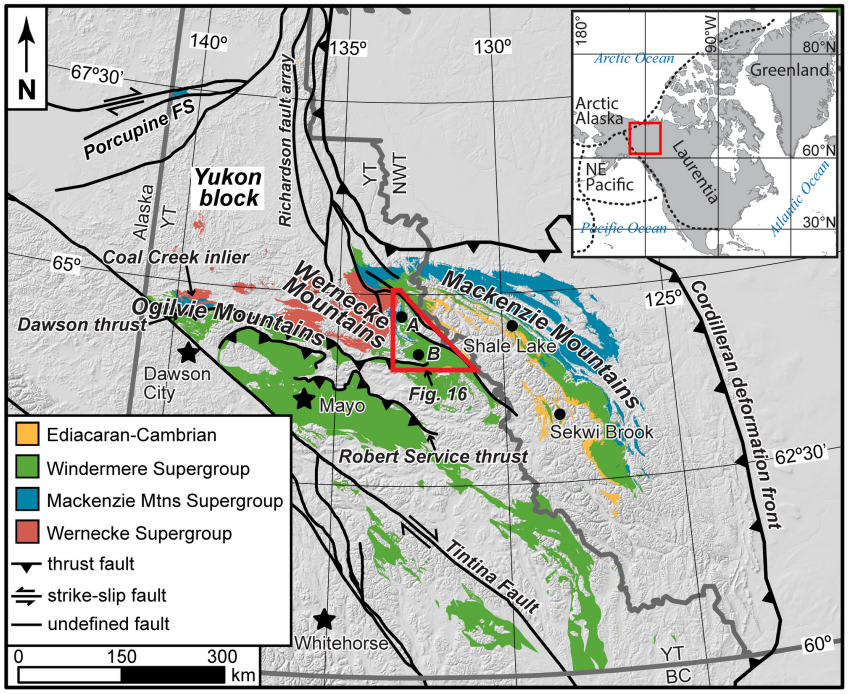

Figure 1. Simplified map displaying the distribution of Mesoproterozoic–early Cambrian strata in northwestern Canada with major structural and paleogeographic elements labeled accordingly. The red polygon outlines the study area presented as a detailed geological map in figure 3. (A) Corn/Goz Creek region; (B) Nadaleen River region. Note: the Ediacaran-Cambrian map unit refers to those formations not currently included in the Windermere Supergroup. Inset map showing major tectonic elements adapted from Gibson et al. (2021). Bedrock geology from the Yukon Geological Survey (2022) and Okulitch and Irwin (2016). Shaded relief elevation data courtesy of the United States Geological Survey (2019). Mtns–Mountains; YT–Yukon Territory; NWT–Northwest Territories; BC–British Columbia; FS–fault system.

Ogilvie Mountains of Yukon (Rooney et al., 2020). There are no geochronological constraints from the Bluefower Fm, but the unconformity that marks the top of the Risky Fm roughly corresponds to the Ediacaran-Cambrian boundary (Aitken, 1989; Kaufman et al., 1997; Narbonne et al., 1994).

The type section of the Gametrail Fm is in the Sekwi Brook region of the Mackenzie Mountains (NWT) where it overlies brown and dark grey turbiditic shale, siltstone, and minor carbonate of the Nadaleen Fm (originally assigned to the Sheepbed Fm; Aitken, 1989; Macdonald et al., 2013). At Sekwi Brook, the Gametrail Fm consists of 322 m of ribbon-bedded lime mudstone, dolostone, and debris-flow breccia/rudstone and records a conformable upper contact with turbiditic shale and sandstone and minor carbonate of the Blueflower Fm (figs. 1, 2; Aitken, 1989). The Gametrail nomenclature was first extended into the Corn/Goz Creek region of the Wernecke Mountains by Aitken (1989) and then expanded to the Nadaleen River area by Moynihan (2014). A graphical summary of the historical nomenclature for the Rackla Group is summarized in table 1. The sedimentology and stratigraphy of the Gametrail Fm in the Wernecke Mountains has been previously documented in the Corn/Goz Creek region, where, despite complications in the original correlation of the Fm between locations (see discussion in Macdonald et al., 2013), large changes in unit thickness and gross sedimentology were identified and interpreted to reflect a depth gradient between the more proximal northern and more distal southern areas (Aitken, 1989; Fritz et al., 1983; Macdonald et al., 2013; Narbonne et al., 1985; Pyle et al., 2004). In the Nadaleen River region of the Wernecke Mountains, the sedimentology and stratigraphy of the Gametrail Fm have been interpreted to represent deposition in a slope environment, suggesting that the shelf-slope transition occurs between the Corn/Goz Creek and Nadaleen River regions (fig. 3; Moynihan et al., 2019).

Contrary to previous work (for example, Aitken, 1989; Fritz et al., 1983; Macdonald et al., 2013; Pyle et al., 2004), we separate the Goz D and F locations (herein referred to as the "Goz D-F block") from the Corn Creek/Goz transect because our revised mapping indicates this area is displaced northwestward by ~30 km of dextral strike-slip motion associated with a prominent splay of the Snake River fault system (fig. 3). As discussed below, this is supported by dramatic shifts in the thickness and lithofacies of the Gametrail Fm, as well as ambiguity in the boundary between the underlying Nadaleen and Ice Brook formations, all of which support separation of the Goz D-F block from the shelf-slope transect.

2. Methods

Field work was undertaken in the Wernecke Mountains over three- to four-week summer field seasons from 2017 to 2019. Nine camps were situated within exposures of the

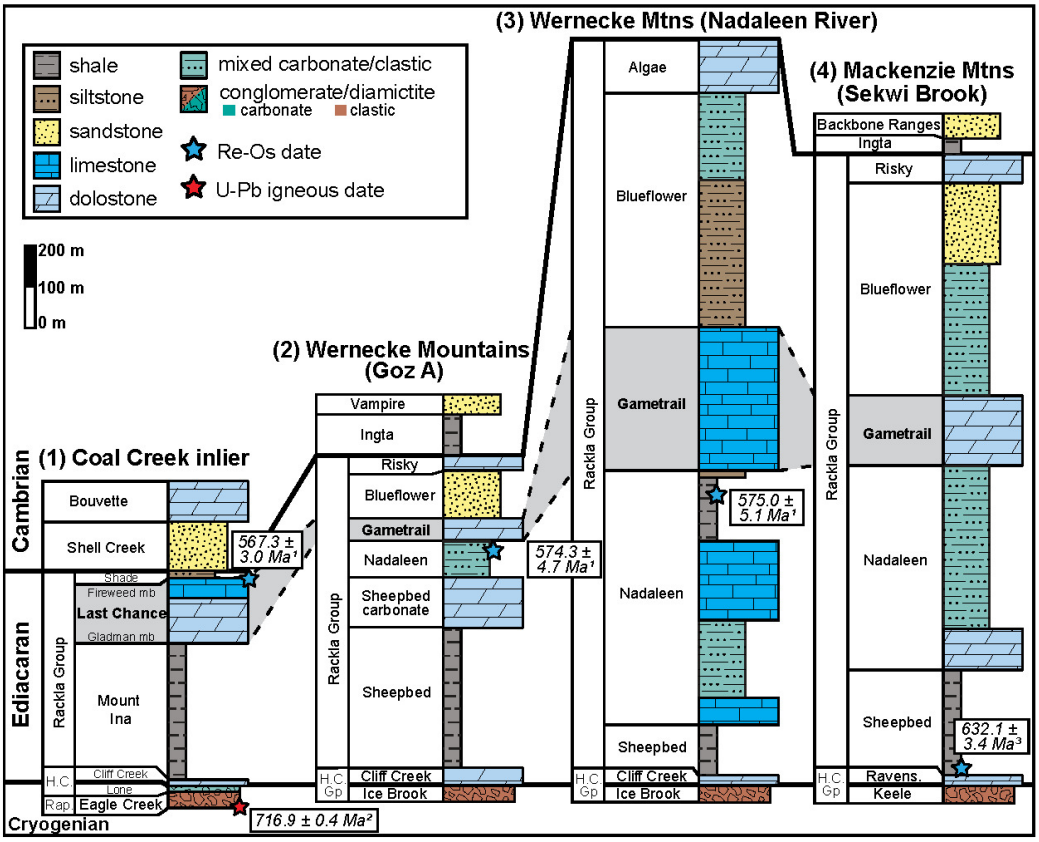

Figure 2. Schematic lithostratigraphic correlation of Cryogenian–Cambrian strata in northwestern Canada modified from Macdonald et al. (2013) and Busch et al. (2021). Note that lithological symbols are reflective of dominant lithologies within each unit. The gray box outlines the proposed correlation of the Gametrail Fm with equivalent strata throughout Yukon and Northwest Territories. The schematic stratigraphic column for the Mackenzie Mountains is after Sekwi Brook, but the Re-Os date is from Shale Lake. [1]Rooney et al. (2020); [2]Macdonald et al. (2010); [3]Rooney et al. (2015). H.C.-Hay Creek; Rap-Rapitan; mb-Member; Gp-Group; Mtns-Mountains; Ravens.–Ravensthroat.

Goz/Corn Creek				Nadaleen River		
					this paper	
Fritz et al. (1983)	Aitken (1989)	Pyle et al. (2004)	Macdonald et al. (2013)	Moynihan et al. (2019)	*Nadaleen River*	*Goz/Corn Creek*
Map unit 11	Risky Formation			Algae Formation		Risky Formation
Unnamed siltstone unit 1						
Unnamed dolostone unit						
Unnamed siltstone unit 2	Blueflower Formation	Blueflower Formation: Disc	Blueflower Formation	Blueflower Formation: Upper	Blueflower Formation	
		Blueflower Formation: Yuletide		Blueflower Formation: Middle		
				Blueflower Formation: Lower	Gametrail Formation	
	Gametrail Formation	Blueflower Formation: Peritidal	Gametrail Formation	Gametrail Formation		
	Sheepbed Formation equivalent	Blueflower Formation: Basal	June Beds	Rackla Group: green siliciclastic	Nadaleen Formation	Nadaleen Formation
				Rackla Group: black shale		
				Rackla Group: upper carbonate		
		Gametrail	Sheepbed carbonate	Nadaleen Formation		
				Rackla Group: heterolithic		
				Rackla Group: lower carbonate		Sheepbed carbonate
	Sheepbed Formation	Sheepbed Formation	Sheepbed Formation	Sheepbed Formation		Sheepbed Formation

Table 1. Correlation chart of historical nomenclature for the Rackla Group in the Wernecke Mountains, Yukon, Canada.

Rackla Group where twelve composite stratigraphic sections of the Gametrail Fm were measured by measuring stick and Jacob staff (coordinates of logged sections are provided in Supplementary Materials S1). In addition to these observational data, we present unpublished (n = 913) and previously published (n = 698; Busch et al., 2022) trace element and carbonate carbon ($\delta^{13}C$), oxygen ($\delta^{18}O$), calcium ($\delta^{44/40}Ca$), and magnesium ($\delta^{26}Mg$) isotope measurements from hand samples collected within these measured sections (geochemical data are presented in Supplementary Materials S2). Here we briefly review the geochemical methodologies, but detailed methods are provided in Supplementary Materials S3 and Busch et al. (2022).

Limestone and dolostone hand samples (0.1-0.5 kg) were collected approximately every meter throughout detailed measured stratigraphic sections and targeted to avoid obvious fracturing or veining. Mineralogy (limestone vs. dolomite) was determined in the field and clean carbonates with minimal siliciclastic components were targeted for geochemistry. The samples were then slabbed perpendicular to bedding using a lapidary saw and ~5-10 mg of powder was drilled from individual laminations using a drill press with a tungsten-carbide drill bit. Unpublished car-

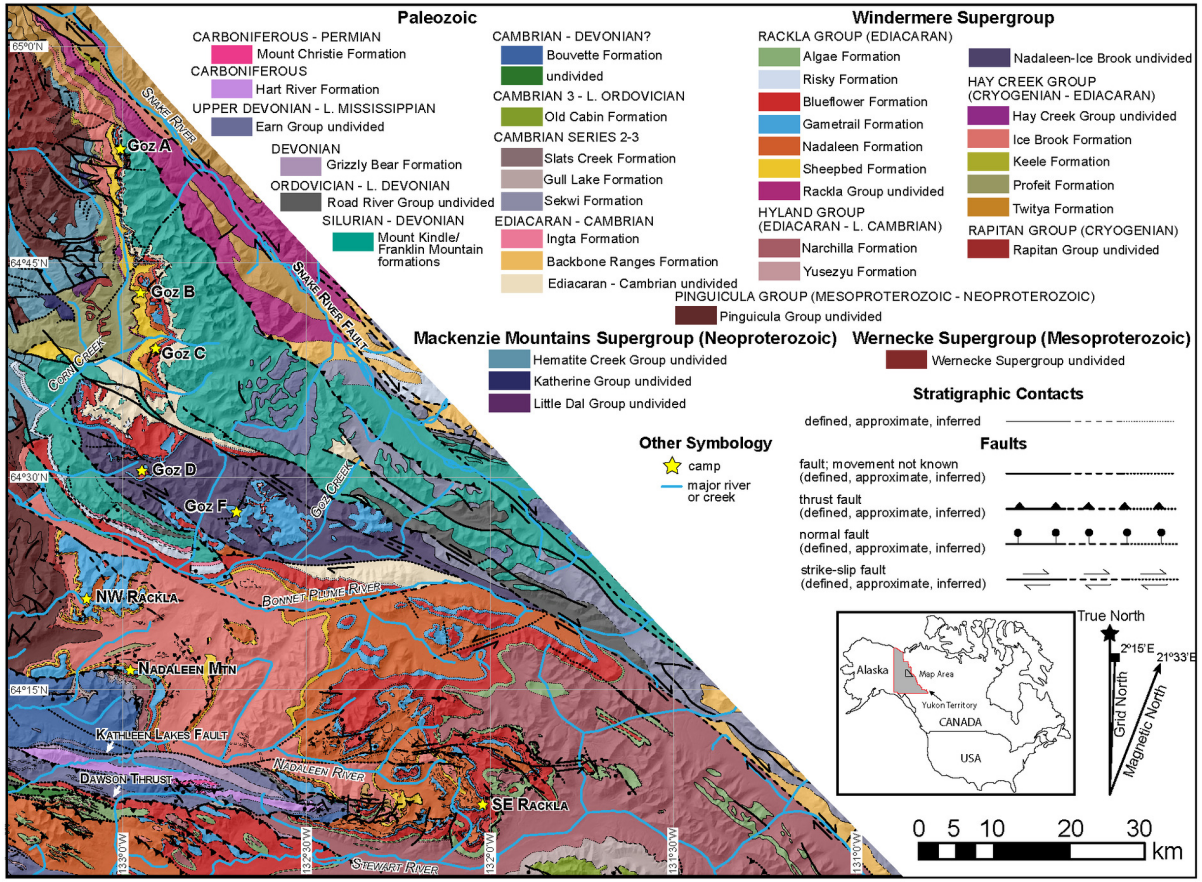

Figure 3. Bedrock geology of the Corn/Goz Creek, Bonnet Plume, and Nadaleen River regions of the Wernecke Mountains, Yukon (NTS 106F, C, B). Mapping includes recent work by the authors and previous work by Blusson (1974), Colpron et al. (2013), Macdonald et al. (2018), Moynihan (2014, 2016), Norris (1982), Roots et al. (1995), and Thorkelson and Wallace (1998); previously published work compiled by the Yukon Geological Survey (2022).

bonate rock samples were analyzed at Dartmouth College for paired $\delta^{13}C$ and $\delta^{18}O$ isotopic measurements following the same methods outlined in Busch et al. (2021, 2022). Carbonate samples were also analyzed at Princeton University for Ca and Mg isotope and trace element analyses following methods outlined in Blättler et al. (2015), Higgins et al. (2018), and Busch et al. (2022).

A new Re-Os date is presented herein from an organic-rich dolostone horizon (JB1714, 31.3 m) that was analyzed at the Yale University Metal Geochemistry and Geochronology Center. Sampling protocols followed methods outlined previously in Strauss et al. (2014) and involved excavating an ~25-cm-deep trench into the outcrop to avoid sampling surficial weathered material, as well as sampling horizontally for up to 65 cm along a single <3-cm-thick horizon to maximize the spread of $^{187}Re/^{188}Os$ values (Kendall et al., 2009). Laboratory methods followed protocols outlined in Rooney et al. (2020). The Re and Os elemental abundances and isotopic data are presented in Supplementary Materials S4.

3. Sedimentology and Lithostratigraphy of the Gametrail Formation

One major challenge that has plagued researchers in attempts at northwestern Canadian Ediacaran lithostratigraphic and chronostratigraphic correlation is the presence of complex siliciclastic-carbonate facies change from shelf to slope localities (table 1; for example, Aitken, 1984, 1989; Fritz et al., 1983; Narbonne et al., 1985). Despite differences in thickness, lithofacies, and exposure/preservation between various localities, the Gametrail Fm can be correlated between the proximal Corn/Goz Creek and distal Nadaleen River areas; however, ambiguities still exist in our understanding of the Goz D-F panel, which will be discussed below. We have grouped our study locations into distinct areas within the shelf-slope transect, primarily based upon similar lithofacies between measured sections. Facies associations (FA) and interpretations for the inferred depositional environments are summarized in table 2. A synthesis of our paleoenvironmental interpretations is presented as a combined sedimentological and sequence stratigraphic model in the Discussion.

The major lithostratigraphic boundaries that we interpret as formational contacts herein are consistent with recent work in the Wernecke Mountains (Macdonald et al., 2013; Moynihan et al., 2019), although below we propose updating the Gametrail-Blueflower formational boundary in the Nadaleen River area from Moynihan et al. (2019) and the Sekwi Brook type area from Aitken (1989). Throughout the study area (fig. 3), basalmost carbonate strata of the Gametrail Fm appear abruptly above various siliciclastic lithofacies of the upper Nadaleen Fm (figs. 4, 5). Although the basal contact is rarely completely exposed, it is inferred to be locally disconformable at Goz A and B due to the presence of a subaerial exposure surface at the formation boundary (fig. 5); the basal contact at Goz C and in the Goz D-F block is unknown due to poor exposure. In the Nadaleen River area (fig. 3), the contact between the upper Nadaleen and Gametrail formations is well-exposed and marked by a gradational and conformable (yet abrupt) change from siliciclastic to carbonate lithofacies (fig. 4C, D). In the Corn/Goz Creek region, the Gametrail-Blueflower formational boundary is commonly marked by a sharp transition into siliciclastic-dominated strata directly above carbonate lithofacies of the upper Gametrail Fm (fig. 4A, B). In the Nadaleen River area, this upper contact is generally well-exposed and characterized by a sharp change from silty limestone to fine-grained siliciclastic strata of the lower Blueflower Fm (fig. 4C). Previously, the Gametrail-Blueflower contact was defined as a vague transition from carbonate- to siliciclastic-dominated strata lower in the succession (previously the lower carbonate member of the Blueflower Fm of Moynihan et al., 2019); here, we propose assigning all these mixed siliciclastic-carbonate strata to the Gametrail Fm so the contact is a more clearly defined lithological boundary (see Discussion).

3.1. Northern Corn/Goz Creek – Nadaleen River shelf-slope transect

3.1.1. Goz A-C: Description

The northern Corn/Goz Creek region includes sites Goz A-C and extends ~27 km along the shelf-slope depositional transect (fig. 5). At Goz A and B, the Gametrail Fm is 80.2 and 113.5 m thick, respectively, while it is 209 m thick at Goz C (fig. 6). At Goz A and B, lowermost Gametrail carbonate strata overlie Nadaleen mixed carbonate-siliciclastic strata with local subaerial exposure surfaces (fig. 7A) and consist of interbedded light grey, fine-grained dolograinstone (FA1), microbialite (FA4), oolitic dolograinstone (FA6), and intraclast rudstone (FA2) that are locally truncated by an erosional surface with up to ~1.4 m of relief (fig. 7B). At Goz B, interbedded dolograinstone and doloboundstone comprising this basal sequence also contain black chert. Above this erosional surface, characteristic orange-tan, hummocky and ripple cross-laminated silty dolograinstone strata of FA1 dominate the lower ~15–50 m of the unit at all sites (FA1; figs. 6, 7E). The bright coloration of FA1 makes the Gametrail Fm an easily identifiable unit throughout the northern Corn/Goz Creek region.

Overlying this FA1-dominated interval, the upper Gametrail Fm becomes characterized by interbedded intraclast rudstone (FA2) and stromatolitic doloboundstone (FA3), especially at Goz A and B. The intraclast rudstone intervals are composed of tabular gravel- to cobble-sized clasts of fine-grained dolograinstone or crystalline dolostone that occur in a silty dolograinstone matrix (fig. 7F), similar to descriptions of carbonate flat-pebble conglomerates (for example, Myrow et al., 2004). Stromatolites are commonly small (~5–10 cm tall and 2.5–5 cm in diameter) and comprised of laterally linked hemispheroidal, nodular, or conical morphologies that often appear to nucleate on top of the intraclast rudstone beds.

At Goz A and B, this interbedded FA 1-2-3 interval gives way to thin- to medium-bedded microbialite (FA4) and occasional large stromatolitic bioherms (FA3) with m-scale domal morphologies (fig. 6). There is a notable lack of stromatolitic doloboundstone at Goz C within this same strati-

Table 2. Summary of Lithofacies in the Gametrail Formation of the Wernecke Mountains, Yukon, Canada.

Lithofacies	Composition	Bedding Style/Structures	Depositional Environment	Distribution
Carbonate Facies:				
FA1: Fine-grained dolograinstone	Tan-orange to grey fine-grained dolograinstone composed of interlocking anhedral crystals of dolomite and minor terrigenous silt; locally includes shale or dolomudstone partings.	Thin- to medium-bedded; generally ripple cross-laminated and occasionally planar-laminated; occasional hummocky or swaley cross-stratification; locally contains Fe-concretions and nodular chert.	Inner to outer ramp subtidal.	Goz A-C.
FA2: Intraclast rudstone	Tan-orange to grey intraclast rudstone with tabular gravel- to cobble-sized subrounded clasts of fine-grained dolograinstone, crystalline dolostone, stromatolitic doloboundstone, or silty limestone; matrix consists of fine-grained silty dolograinstone, dolomudstone, or silty limestone.	Thin- to thick-bedded; occasionally base of beds scour into underlying strata; locally interbedded with fine-grained dolograinstone and/or stromatolitic doloboundstone. Commonly associated with soft sediment deformation in deeper-water settings.	Inner to outer ramp subtidal or slope.	Goz A-D, Nadaleen River region.
FA3: Stromatolitic doloboundstone	Light to dark grey, tan-orange, or maroon stromatolitic doloboundstone; stromatolite morphologies include laterally linked hemispheroidal, nodular, and conical in both low- and high-inheritance forms; stromatolites occasionally nucleate on top of intraclast rudstone beds. Also comprise large, m-scale domal bioherm constructions.	Stromatolites range from ~5–20 cm in height and ~2.5–20 cm in diameter; often interbedded with intraclast rudstone and fine-grained dolograinstone in ~0.5–2 m thick parasequences; locally contains vuggy or sparry diagenetic textures; bioherms range from 25 cm to 1 m in height and 25 cm to 1.5 m in diameter; locally contain a clotted, irregular fabric.	Inner to outer ramp subtidal.	Goz A, B, D, F.
FA4: Microbialite	Light to dark grey planar to wavy laminated doloboundstone; distinguished from FA3 by crinkly, flat laminations and lack of synoptic relief.	Thinly laminated and wavy or irregular ("crinkly") planar laminations; beds are commonly ~0.5 to 1.5 m thick.	Inner to outer ramp subtidal or lagoonal.	Goz A-D, Nadaleen River region.
FA5: Coated grain dolo-packstone/ wackestone	Light to dark grey packstone and wackestone dominated by coated grains; clasts are generally thin, elongate cortoids ranging from 2 to 20 mm in length and are mostly locally-derived microbialite or stromatolite; locally clasts include gravel-sized aggregates; matrix is composed of dolomudstone.	Thin- to thick-bedded; generally cross-bedded at the ripple- to dune-scale; contains tabular and lenticular bedding configurations; beds are often normal graded; locally contains vuggy or sparry diagenetic textures.	Inner to outer ramp subtidal or lagoonal.	Goz D and F.
FA6: Pisolitic/ oolitic dolograinstone	Light grey pisolitic or oolitic grainstone; grains subrounded to well-rounded and well- to poorly-sorted; occasionally contain granule- to pebble-sized aggregate grains; matrix composed of dolomite spar or medium- to very coarse-grained quartz sand.	Thin- to thick-bedded; generally trough cross-stratified; tabular and lenticular bedding configurations; occasionally interbedded with stromatolitic doloboundstone; locally contains vuggy or sparry diagenetic textures.	Intertidal to subtidal shoal complex.	Goz A and F.
FA7: Lime-/dolomudstone	Light grey to orange lime-/dolomudstone; often interbedded with FA2 and FA8 at the cm-scale; breaks with a characteristic conchoidal fracture.	Thin- to thick-laminated; generally planar; often occurs as the final subdivision in a partial or full Bouma sequence; locally contains soft sediment deformation.	Outer ramp subtidal to Slope.	Goz C and the Nadaleen River region.
FA8: Silty limestone	Tan, maroon, or grey-green silty limestone; composed of interlocking crystals of anhedral calcite with terrigenous silt and rare euhedral dolomite; sometimes interbedded with FA2; silty limestone can be silt- or carbonate-dominated.	Thin-laminated and thin-bedded; often planar with partial to full Bouma sequences; locally contains pyrite which stains outcrop with Fe-oxides; locally contains soft sediment deformation, including chaotic bedding, slump folds, flame structures, and load casts.	Outer ramp subtidal to slope.	Restricted to the Nadaleen River region.
FA9: Sandy lime-/dolostone	Tan to orange sandy dolostone or grey-green sandy limestone; sand- to granule-sized dolograinstone with fine- to medium-grained quartz and/or lithic clasts; clasts display moderate sorting and are subangular to well-rounded; locally contains rip-up clasts	Thin- to medium-bedded; generally trough cross-stratified or ripple cross-laminated; rarely contains hummocky cross-stratification; locally contains lenses of silty dolograinstone.	Outer ramp subtidal to slope.	Goz C, NE Rackla, and Nadaleen Mtn.

Lithofacies	Composition	Bedding Style/Structures	Depositional Environment	Distribution
	of dolograinstone; matrix is silty dolograinstone or calcareous siltstone.			
Diagenetic Facies:				
FA10: Crystalline dolostone	Light grey or maroon crystalline dolostone; composed of anhedral to euhedral crystalline dolomite spar; locally associated with FA14.	Generally thick-bedded and massive with little to no preservation of carbonate textures or sedimentary structures; locally contains fenestral and/or zebra dolomite textures, as well as Fe-oxide or distinct maroon staining.	Inner ramp subtidal or lagoonal; mid-outer ramp subtidal.	Goz A-D.
Siliciclastic Facies:				
FA11: Shale	Dark grey to black fissile shale.	Fissile.	Inner to outer ramp subtidal.	Restricted to Goz C.
FA12: Siltstone	Dark grey to brown siltstone.	Occurs as thin drapes on sandstone beds of FA13.	Inner to outer ramp subtidal.	Goz C and SE Rackla.
FA13: Sandstone	Dark grey, brown, or orange lithic arenite; fine- to very coarse-grained quartz and lithic fragments of shale and carbonate; subangular; poorly-sorted.	Thin- to medium-bedded; ripple cross-lamination and trough cross-stratification; lenticular bedding configurations; interbedded with FA11 and FA12.	Inner to outer ramp subtidal.	Restricted to Goz C.
FA14: Pebble Conglomerate	Light grey to tan matrix-supported pebble conglomerate; clasts are granule- to gravel-sized and composed of quartzite, chert, dolograinstone, and crystalline dolostone; subrounded to subangular; poorly-sorted; matrix composed of medium- to coarse-grained sandy dolograinstone and spar.	Occurs as laterally discontinuous to vertical pipes within stromatolitic bioherms and other carbonate facies; no discernable internal sedimentary structures.	Associated with subaerial exposure surface and filled paleokarst cavities.	Restricted to Goz A and B.

graphic interval; instead, it is dominated by intraclast rudstone (fig. 6). Goz C also contains a prominent 20.3 m thick interval of massive crystalline dolostone composed of anhedral to euhedral dolomite with abundant void- and fracture-filling euhedral quartz veins, followed by a recessive interval and interbedded silty dolograinstone and sandy dolostone unit (FA9; fig. 6).

At all locations in this northern part of the transect, there is a prominent stratigraphic boundary towards the upper part of the Gametrail Fm above which strata are either poorly exposed, composed of crystalline dolostone with little to no preservation of carbonate textures, or comprised of nodular to concretionary microbialite or stromatolitic doloboundstone (fig. 6). At Goz A, this stratigraphic boundary (~50 m in JB1706/JB1707)) is locally marked by a 6.4 m deep subvertical pipe of matrix-supported pebble conglomerate (FA13) composed of poorly sorted, subrounded to subangular, granule- to cobble-sized clasts of quartzite, dolograinstone, and crystalline dolostone set in a medium- to coarse-grained sandy dolograinstone matrix (fig. 7D). Along strike, isolated pods of this conglomerate and minor sandstone occur sporadically throughout the host carbonate strata. This interval at Goz B (~85 m in JB1713) is represented by a 1.5 m thick interval of coarsely crystalline dolostone before an abrupt transition into recessive, poorly exposed black shale (FA11; fig. 6). Laterally along this surface, we have recognized m-scale topographic relief along this surface (fig. 7C), as well as similar subvertical pipes and irregular pods composed of matrix-supported conglomerate. At Goz C (~160 m in JB1822), there is a distinctive 5.4 m thick interval of poorly sorted trough cross-stratified sandy dolostone (FA9) with resedimented carbonate clasts before a transition into ~6 m of interbedded shale, siltstone, and sandstone (FA11-13; fig. 6).

3.1.2. Goz A-C: Interpretation

The Gametrail Fm of the Wernecke Mountains has commonly been interpreted as recording marine storm-dominated carbonate ramp sedimentation (Busch et al., 2022; Macdonald et al., 2013; Pyle et al., 2004). Lowermost Gametrail Fm carbonate strata at Goz A-B directly overlie Nadaleen Fm strata with prominent mudcracks (fig. 7A), signifying that local subaerial exposure of unknown duration occurred prior to marine flooding in these shallowest settings. The presence of oolitic dolograinstone in the directly overlying and lithologically diverse lower part of the Gametrail Fm at Goz A-B likely confirms deposition in a shallow-water inner ramp setting, as the formation and deposition of ooids preferentially occurs in high-energy subtidal to intertidal environments (for example, Diaz & Eberli, 2019). The common occurrence of intraclast rudstone, or flat-pebble conglomerate, throughout the Goz A-C panel, but in greater abundance at Goz C, also suggests consistent deposition above storm wave base, as they are commonly thought to form during storm wave action or reworking of shoreline deposits in peritidal or subtidal settings (for example, Myrow et al., 2004). Storm-influenced inner to outer

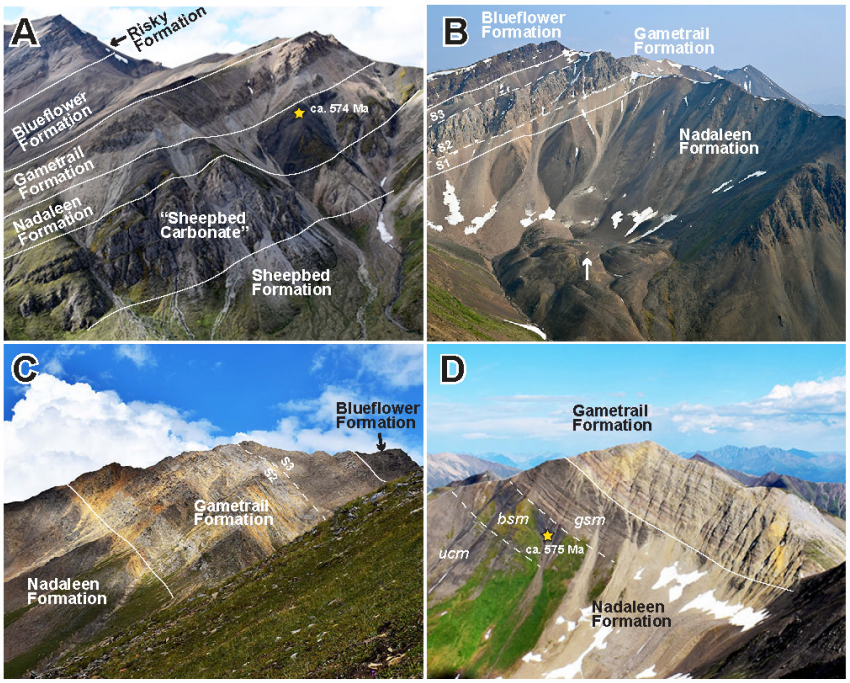

Figure 4. Photographs of selected localities from the northern Corn/Goz Creek and Nadaleen River regions. (A) Image looking southeast at the Rackla Group of Goz A. Yellow star indicates location of Re-Os date shown in figure 2; Nadaleen Fm is 87.5 m thick for scale. (B) Image looking southeast at the Rackla Group of Goz B. Note the significant thickness increase and change in outcrop character in the Nadaleen Fm compared to Goz A. Tents are arrowed for scale and the S1-3 depositional sequences are labeled in the Gametrail Fm. (C) Typical outcrop style of the Gametrail Fm in the Nadaleen River area. The S2 and S3 depositional sequences are labeled accordingly in the Gametrail Fm and it is locally ~265 m thick for scale. (D) Image looking east at the Gametrail Fm in the southern Nadaleen River area (Section G2 of Moynihan et al., 2019). Yellow star indicates the interval sampled for Re-Os geochronology (fig. 2) in the black shale member (bsm) of the Nadaleen Fm. Also shown are boundaries between the upper carbonate member (ucm) and green siliciclastic member (gsm) of the Nadaleen Fm.

ramp sedimentation is also consistent with the presence of hummocky and ripple cross-stratification throughout the bulk of the Gametrail Fm in these locations (fig. 7E). The interbedded microbialite, stromatolitic doloboundstone, and crystalline dolostone in the uppermost Gametrail Fm at Goz A and B (fig. 6) could reflect an up-section transition to peritidal sedimentation, as the association of microbialite and vuggy dolostone is a characteristic feature of peritidal carbonate deposits (James & Wood, 2010); however, the lack of clear subaerial indicators and dominance of stromatolitic and cross-laminated dolograinstone facies (fig. 6) more likely indicates a consistent inner-middle ramp setting with background quiescent sedimentation punctuated by storm events. Broadly, the greater abundance of shallow marine subtidal to intertidal lithofacies and the thinner expression of the Gametrail at Goz A-B (~80–115 m) compared with Goz C (~210 m) confirms a deepening direction to the south in the Corn/Goz Creek region (figs. 5, 6; Pyle et al., 2004).

There are at least three depositional sequences separated by subaerial exposure surfaces in the Gametrail Fm at Goz A-C. The first sequence boundary is well-exposed at Goz A-B where it is characterized by an irregular erosional surface that truncates the lithologically diverse lower part of the Gametrail Fm (fig. 7B), sharing many characteristics with "scalloped" erosional features documented in other subaerial exposure surfaces on carbonate platforms (for example, Read & Grover, 1977). This lower sequence boundary is either absent or covered at Goz C (fig. 6). The second sequence boundary is manifest by the prominent lithological breaks and localized subvertical pipes and pockets of matrix-supported pebble conglomerate at Goz A-B (fig. 7C, D), the latter of which has the characteristic composition and morphology of filled paleokarst voids and breccia pipes (for example, Maslyn, 1977). This second sequence boundary is also represented by a sharp transition to crystalline vuggy dolostone locally around Goz B that is interpreted to reflect early diagenetic fabric-destructive dolomitization, potentially in the mixing zone between marine and meteoric groundwater in the phreatic zone (for example, Badiozamani, 1973). At Goz C, this surface is represented by the appearance of sandy dolostone with both resedimented carbonate clasts and coarse-grained quartz sand higher in the section (fig. 6) that likely indicates shoaling into an emergent setting. The recessive interval of poorly exposed black shale and siltstone above the second sequence boundary at Goz B-C (fig. 6) probably represents deepening into a lagoonal or protected subtidal environment. Finally, the

uppermost carbonate interval dominated by concretionary microbialite/stromatolitic doloboundstone and crystalline dolostone (fig. 6) at Goz A-C indicates a third shoaling sequence into an emergent and/or peritidal environment beneath the subaerial exposure surface that marks the Gametrail-Blueflower contact.

3.1.3. Nadaleen River: Description

The Nadaleen River region (figs. 3, 8) includes three sites located along or adjacent to the Rackla belt, an east-west trending Carlin-type gold mineralization zone between the Dawson Thrust and Kathleen Lakes Fault (Moynihan et al., 2019; Pinet et al., 2022; Tucker et al., 2012). Within this region, there are two distinct lithological domains that will be discussed separately: 1) the NW Rackla and Nadaleen Mountain locations, and 2) the SE Rackla section (fig. 6). The latter is in proximity to measured sections G1, G2, and G3 of the Gametrail Fm described in Moynihan et al. (2019).

The NW Rackla and Nadaleen Mountain sites share many similarities and are separated by only ~10 km (figs. 6, 8–9). The basal contact with the Nadaleen Fm at the NW Rackla site is marked by an abrupt shift from interbedded siltstone and fine-grained sandstone to monotonous grey-green calcareous siltstone (FA8; fig. 6). At Nadaleen Mountain, the boundary is characterized by an abrupt contact between calcareous black shale and matrix-supported rudstone with lime mudstone clasts in a sandy limestone matrix (FA2; fig. 6). The thickness of the Gametrail Fm in this region ranges from 220–265.6 m, and it is largely dominated by maroon to green calcareous siltstone that is often interbedded with lime mudstone (FA8). This facies contains abundant partial (primarily T_{cde}) to full Bouma sequences and soft sediment deformation, including slump folds and chaotic bedding, in addition to intraformational truncation surfaces (fig. 6). Although the sections in this domain are dominated by FA8, there are isolated instances of stratiform to lenticular intraclast rudstone beds with tabular subrounded pebble to cobble-sized clasts of lime mudstone set within a tan silty matrix (FA3) and fine- to coarse-grained sandy limestone with abundant ripple cross-lamination (FA9; fig. 6). There is no discernable stratigraphic trend in the progression of carbonate lithofacies from the base to the top of the Gametrail Fm at these locations (fig. 6). At NW Rackla, the upper contact with the Blueflower Fm is not exposed, while at Nadaleen Mountain the contact is covered (fig. 6).

The SE Rackla site is located over 50 km from the NW Rackla and Nadaleen Mountain localities and marks a discernable difference in the recorded lithofacies (figs. 6, 8). Moynihan et al. (2019) also noted a distinct E-W transition in carbonate lithofacies within the Nadaleen River area, and our SE Rackla section is close to their G2 and G3 measured sections (fig. 8). The SE Rackla section is a similar thickness (294.4 m) to the G2 and G3 sections of Moynihan et al. (2019), and the basal contact with the Nadaleen Fm is characterized by an abrupt change from fine- to medium-grained sandstone and siltstone to ~3 m of orange-weathering thin-bedded lime mudstone (FA7). Above this basal interval, there is ~8 m of interbedded lime mudstone and green-grey calcareous siltstone with rare Bouma T_{cde} subdivisions and flute casts (FA8; figs. 6, 9C). Until the upper ~90 m of the section, these strata are dominated by silty limestone (FA8) and lime mudstone with infrequent partial Bouma sequences (fig. 9A, B). Interspersed throughout the lower part of the section there are rare slump folds, thicker

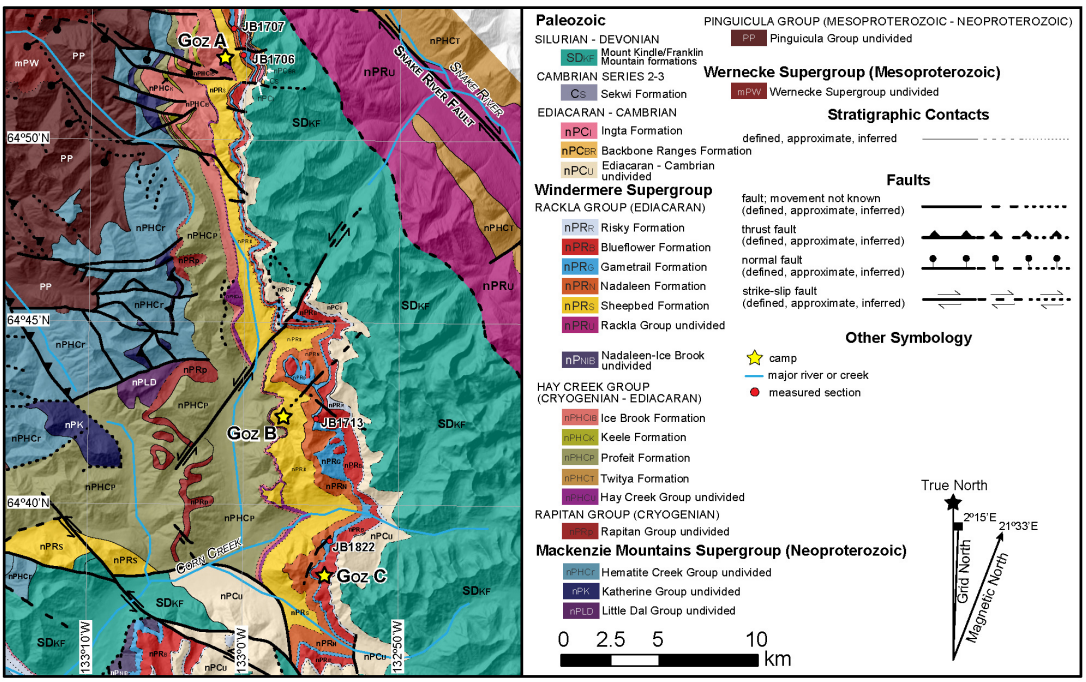

Figure 5. Bedrock geology of the northern Corn/Goz Creek region of the Wernecke Mountains, Yukon. Measured stratigraphic sections are plotted as red circles and presented in figure 6.

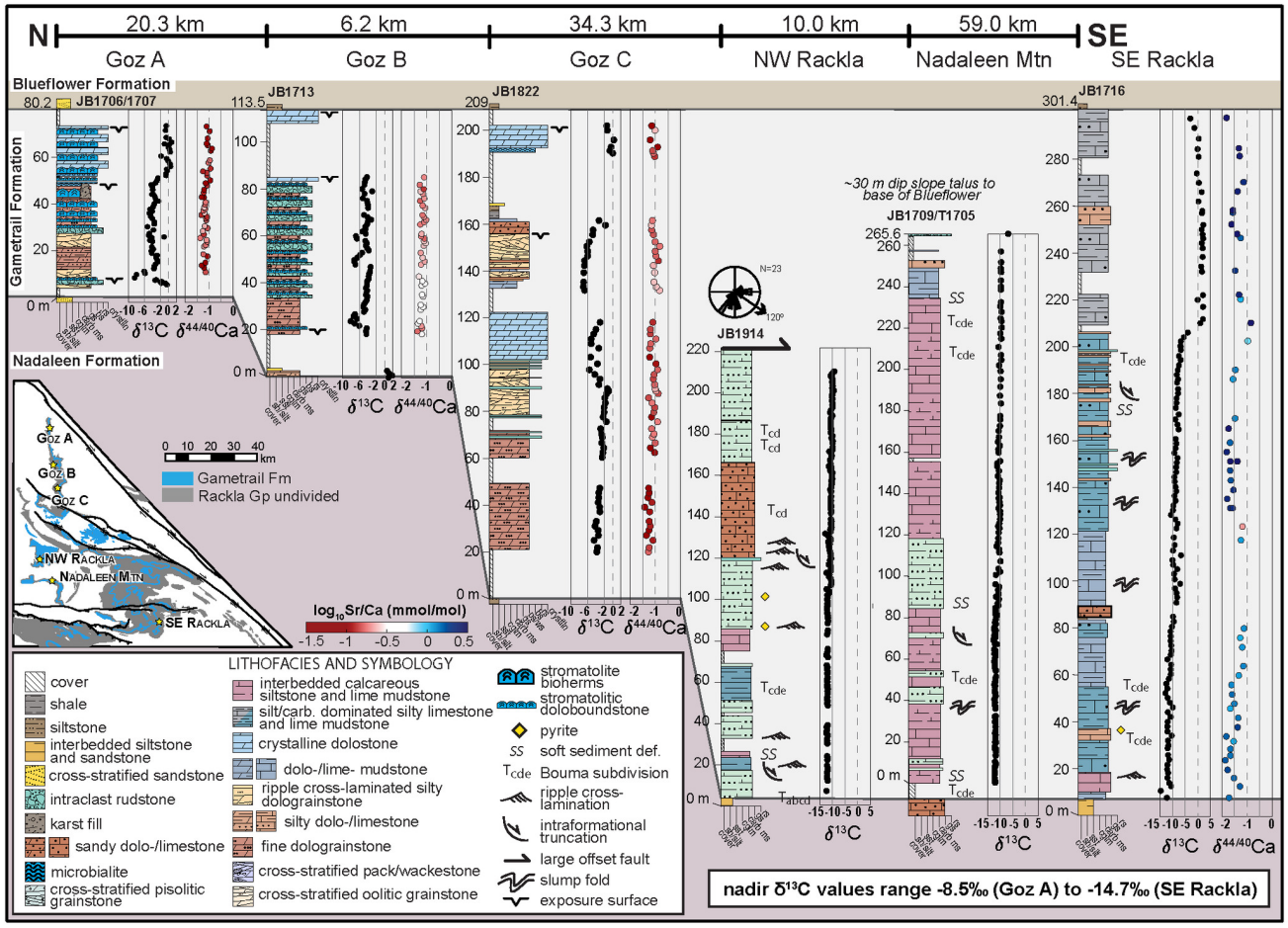

Figure 6. Detailed measured sections and carbon and calcium isotope stratigraphy of the Gametrail Fm across a shelf-slope depositional transect between the northern Corn/Goz Creek and Nadaleen River regions of the Wernecke Mountains, Yukon. Inset map on the left depicts the location of each measured section. Calcium isotope data is colored by the $log_{10}Sr/Ca$ ratios (mmol/mol). Dip-corrected paleocurrent data from the NW Rackla location is plotted as a rose diagram (arrow indicates the mean vector). sh-shale; silt-siltstone; sst-sandstone; cglm-conglomerate; carb ms-carbonate mudstone; gs-grainstone; bs-boundstone; rs-rudstone; crystlln-crystalline.

intervals of tan silty limestone (FA8), and localized zones of silicification (figs. 6). Between ~150 and 200 m there are frequent intervals of intraclast rudstone composed of granule- to cobble-sized tabular clasts of lime mudstone in a tan silty limestone matrix that often fines upwards (FA2; figs. 6, 9D). Slump folds and convolute bedding, as well as an intraformational truncation surface, were also observed in this interval. There is a distinct boundary at ~210 m, which is recorded by a facies transition to silt-dominated silty limestone interbedded with lime mudstone (figs. 4C, 6); this was previously considered the Gametrail-Blueflower Fm contact. We suggest the upper contact with the Blueflower Fm is instead marked by a more obvious and abrupt shift from interbedded lime mudstone and silty limestone to fissile siltstone and shale.

3.1.4. Nadaleen River Area: Interpretation

Lithofacies observed in the Nadaleen River region broadly support previous interpretations for deposition in a slope setting (Moynihan et al., 2019). The preponderance of fine-grained lithologies, abundant normal grading, and full to partial Bouma sequences suggest an environment dominated by suspension and sediment gravity sedimentation below maximum storm wave base (Bouma, 1962). The presence of abundant soft-sediment deformation and rare intraformational truncations are also diagnostic of a slope environment (for example, Playton et al., 2010). Furthermore, the common occurrence of matrix- and clast-supported intraclast rudstone in these successions are interpreted as debris flow or slump deposits with clast lithologies that suggest they were locally derived from the shelf and/or slope system (for example, Moscardelli & Wood, 2008). The prominent influx of terriginous silt towards the top of the Gametrail Fm at the SE Rackla location (~210 m; fig. 6) and other sections described by Moynihan et al. (2019) could indicate a shoaling from the toe of slope or middle slope to the upper slope, but this is not entirely diagnostic and could result from upslope sediment delivery dynamics. Longitudinal differences in lithofacies could suggest lateral heterogeneity in the slope environment or differences in water depth (fig. 6). For example, overall coarser-grained lithofacies and more abundant density and turbidity currents at the NW Rackla and Nadaleen Mountain sites (fig. 6) could indicate a position within a toe of slope channel-levee complex that funneled coarser material towards the basin floor. However, due to the large distances between the measured stratigraphic sections and our lack of sedimentological data between them, it is not possible to assign these lateral differences to specific environments within the overall slope depositional system.

3.2. Goz D-F block

3.2.1. Goz D: Description

Goz D records a striking difference in lithofacies from the northern Corn/Goz Creek and Nadaleen River locations discussed above. Within the Goz D area, there is also significant variation in unit thicknesses and lithofacies, even in locations separated by a few kilometers (fig. 10; Pyle et al., 2004), which is suggestive of a more complex depositional setting. Given the complex nature of the inferred depositional system, it is possible that the regional chronostratigraphic correlation of these strata, which have herein been assigned to the Gametrail and Blueflower formations following Pyle et al. (2004) and Macdonald et al. (2013), will need to be further modified (see Discussion).

There are two distinct lithological domains among our five measured stratigraphic sections of the Gametrail Fm in the Goz D area that will be discussed separately: 1) multiple sections dominated by cross-stratified coated grain packstone, wackestone, and grainstone (FA5), and 2) a section dominated by decameter-thick stromatolitic bioherms. The first lithological domain is represented by the northwestern-most and southwestern-most measured sections (JB1817/18, JB1820, JB1821, JB1714/1816; figs. 10, 11) where the exposed Gametrail Fm is 82.9–173.3 m thick and the basal contact with the underlying siliciclastic unit (Nadaleen/Ice Brook undivided) is covered. These sections commence with thin-bedded trough cross-stratified coated grain pack-/wackestone (FA5) that is interbedded with dolomudstone (FA7) and microbialite (FA4; fig. 11D). The microbialite facies comprise much of the basal Gametrail Fm in this area (fig. 10) and are locally associated with stromatolitic doloboundstone (FA3). Above this lower interval, most sections are dominated by interbedded coated grain pack-/wackestone, crystalline dolostone (FA10), and stromatolitic doloboundstone (fig. 10). The pack-/wackestone intervals are commonly trough cross-stratified with elongate aggregate clasts that range from 2–10 mm. Towards the top of sections JB1817/18, JB1820, and JB1821, there are ~2–11 m thick intervals of stromatolitic doloboundstone (FA3), which are either preserved as m-scale domal stromatolitic bioherms or cm-scale stromatolites interbedded with reworked doloboundstone intraclasts and local vuggy textures (fig. 10). In contrast, the upper portion of section JB1714/1816 is dominated by ~1.4–10 m thick packages of medium-bedded, matrix-supported intraclast rudstone with gravel- to cobble-sized sub-rounded clasts of doloboundstone (FA2; fig. 10). Where exposed, the uppermost beds of the Gametrail Fm in these sections contain a fenestral or vuggy texture with localized brecciation and abundant ferruginous carbonate or oxide cements.

The second lithological domain is captured in a single 95.8 m thick stratigraphic section (JB1815) in the central part of this area that is dominated by spectacular amalgamated stromatolitic bioherms with significant synoptic relief (figs. 10, 11B). The base of the Gametrail Fm is not exposed at this locality, but the section begins with interbedded dolomudstone (FA7) and cross-stratified coated grain pack-/wackestone (fig. 10). This is succeeded by an interval of stromatolitic doloboundstone with hemispheroidal stromatolites (~2 cm in diameter) and microbialite interbedded with trough cross-bedded coated grain packstone (fig. 10). A 4.2 m thick occurrence of thick-bedded clast-supported intraclast conglomerate appears above this basal sequence with granule- to cobble-sized, subangular to subrounded clasts of coated grain pack-/wackestone within

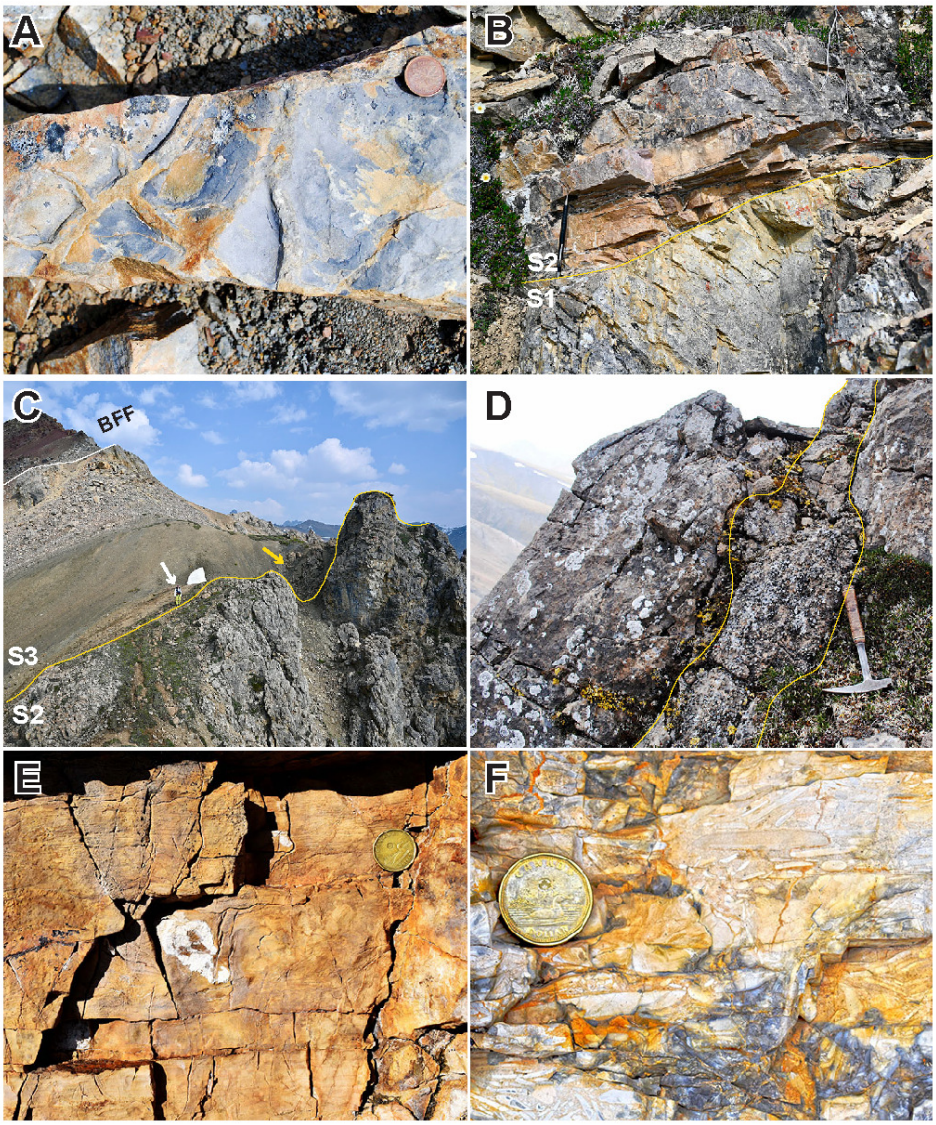

Figure 7. Photo panel of representative lithofacies and stratigraphic relationships from the Gametrail Fm in the northern Corn/Goz Creek region. (A) Mudcracks along a bedding surface of interbedded calcareous siltstone and sandstone at the contact between the Nadaleen and Gametrail formations at Goz A. Coin is 1.9 cm in diameter. (B) Erosional contact (yellow line) between grey stromatolitic doloboundstone (FA3) and tan cross-laminated silty dolograinstone (FA1) marking the S1-S2 sequence boundary at Goz B. Pencil is 14 cm long. (C) Relict paleokarst topography at the S2-S3 sequence boundary (yellow line) at Goz B. Yellow arrow depicts distinct karst breccia fill and white star outlines geologist for scale; BFF–Blueflower Fm. (D) Paleokarst cavity (outlined in yellow) filled with granule- to cobble-sized clasts of carbonate, chert, and quartzite in a carbonate-cemented quartz sand matrix (FA14) within vuggy recrystallized dolostone (FA10) of the upper Gametrail Fm at Goz A. Rock hammer is 33 cm long. (E) Characteristic tan-orange ripple cross-laminated silty dolograinstone (FA1) interbedded with microbialite (FA4) in the lower Gametrail Fm at Goz B. Coin is 2.7 cm in diameter. (F) Intraclast rudstone (FA2) composed of tabular pebble/cobble dolograinstone clasts in a silty dolograinstone matrix from the lower Gametrail Fm at Goz A. Coin is 2.7 cm in diameter.

a dolomudstone matrix that laterally transitions into stromatolitic bioherms (fig. 10). The remainder of the section is dominated by amalgamated stromatolitic bioherms characterized by m-scale domal morphologies with crinkly and irregular laminae, as well as intervals of vuggy, clotted, or fenestral textures (fig. 10). In some instances, there are ferruginous cements and laminae within individual stromatolites in these buildups (fig. 11C), and locally, there are smaller conical, planar, or hemispheroidal stromatolites within the larger bioherms. Based on lateral measured sections (JB1819), the examined stromatolitic buildups have at least ~35 m of synoptic relief, as they strike laterally into fine-grained siliciclastic strata of the lower Blueflower Fm (figs. 10, 11B). The uppermost beds of the Gametrail Fm in this section are marked by a zone of brecciation and infilled voids composed of carbonate mud, vuggy textures,

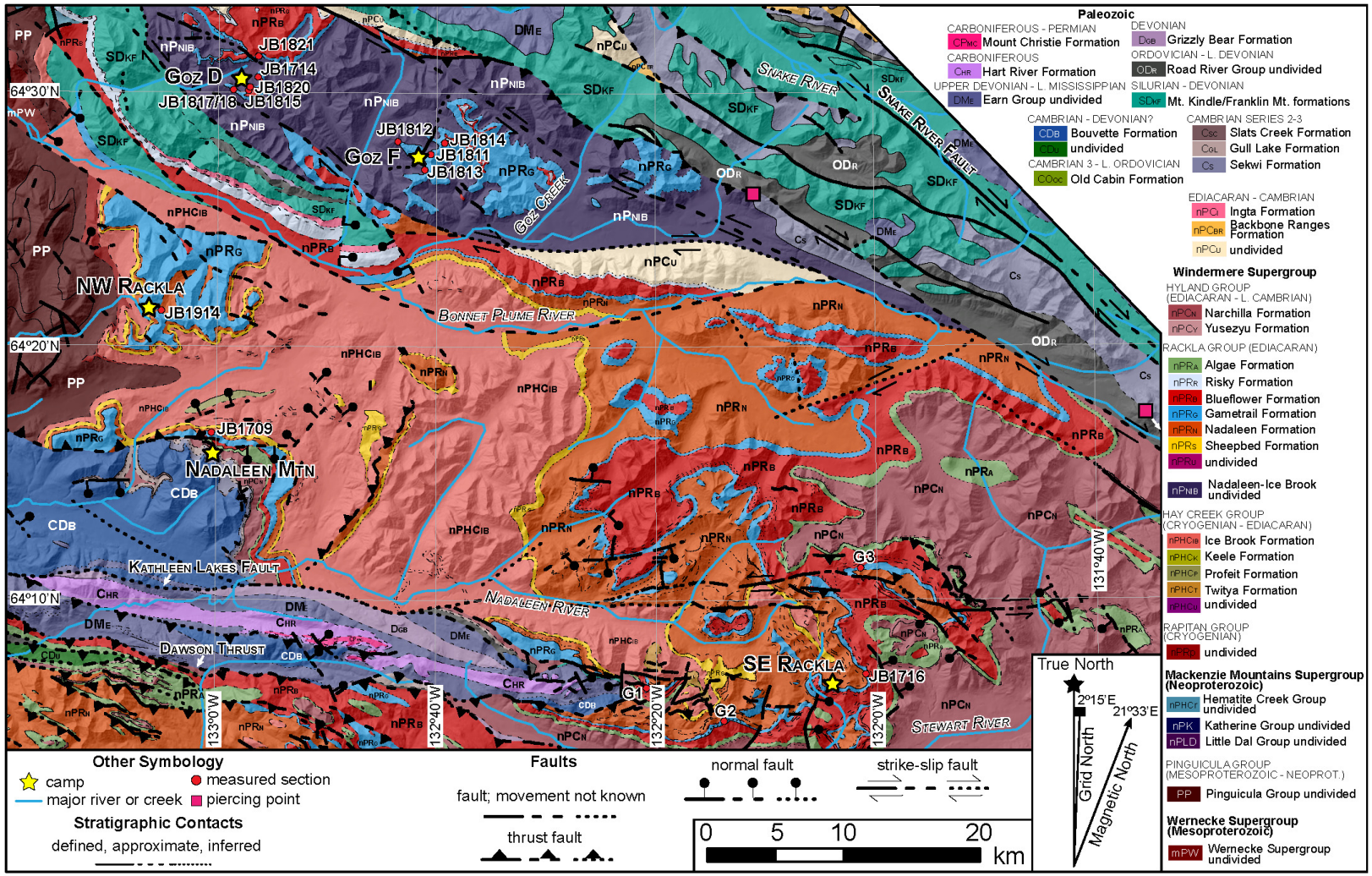

Figure 8. Bedrock geology of the southern Corn/Goz Creek and Nadaleen River regions of the Wernecke Mountains, Yukon. Stratigraphic sections are plotted as red circles and presented in figures 6 and 10. There is an estimated 30 km of dextral displacement along the strike-slip faults which bound the Goz D-F block, with the Sekwi Fm interpreted as a piercing point on displacement (pink squares) for palinspastic restoration. Sections G1, G2, and G3 from Moynihan et al. (2019) are also shown for reference.

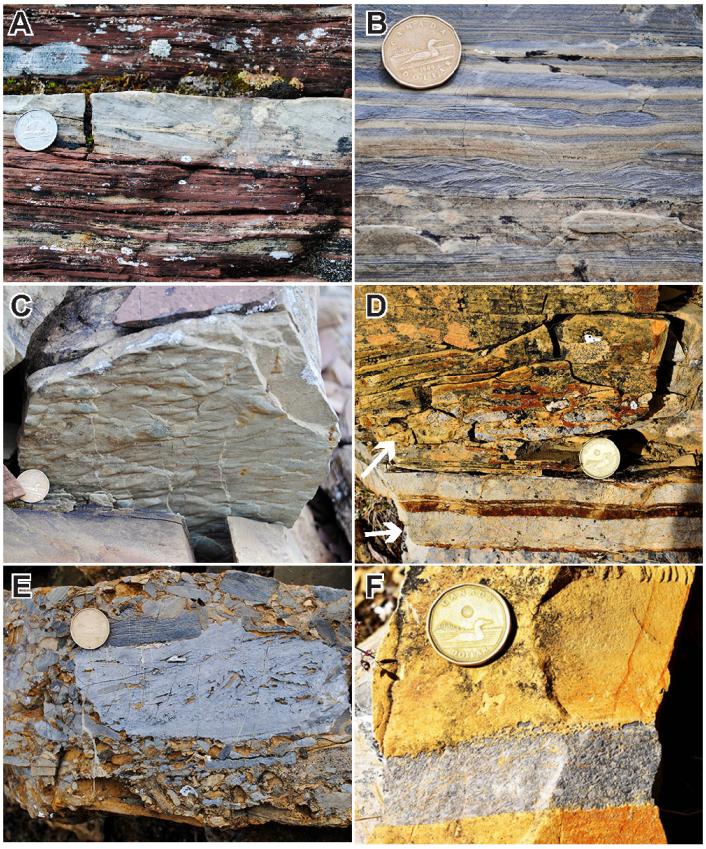

Figure 9. Photo panel of representative lithofacies from the Gametrail Fm in the Nadaleen River region. (A) Distinctive maroon- and grey-weathering thin-bedded silty limestone (FA8) turbidites with partial Bouma Tcde and Tde subdivisions. Coin is 2.1 cm in diameter. (B) Characteristic tan- and grey-weathering thin-bedded silty limestone (FA8) common throughout the Nadaleen River area with partial Bouma Tcde subdivisions. Coin is 2.7 cm in diameter. (C) Flutes on the sole of a fine-grained sandstone bed from the siliciclastic-rich upper part of the Gametrail Fm. Coin is 2.7 cm in diameter. (D) Successive interbeds of intraclast rudstone (indicated by white arrows) composed of grey tabular gravel- to cobble-sized clasts of lime mudstone in a tan silty limestone matrix (FA2) from JB1716. Note how the lower bed is clast-supported, while the upper bed is matrix-supported. Coin is 2.7 cm in diameter. (E) Polymict intraclast rudstone with gravel- to cobble-sized clasts of grey lime mudstone and tan silty limestone in a silty limestone matrix (FA2). Coin is 2.7 cm in diameter. (F) Normal-graded coarse-grained wackestone composed of sand- to granule-sized subrounded clasts of lime mudstone in a silty limestone matrix from JB1716. Coin is 2.7 cm in diameter.

and botryoidal cements with a bright maroon coloration. The upper contact with the Blueflower Fm is locally covered, but lowermost exposures of the siliciclastic rocks consist of thin- to medium-bedded quartz arenite with lenticular bedding (fig. 10).

3.2.2. Goz D: Interpretation

Gametrail Fm carbonate lithofacies in the Goz D region broadly represent deposition within and adjacent to at least one prominent stromatolite patch reef system, a setting that was also recognized by Pyle et al. (2004). The abundant cross-stratified coated grain wackestone and packstone in adjacent sections are interpreted to represent subtidal deposits, where clast material was locally derived from the stromatolite buildups and could indicate the patch reefs were situated in a high-energy shallow-water setting (for example, James & Wood, 2010). The intervals dominated by microbialite are interpreted to reflect sedimentation in a more quiescent or protected environment adjacent to the large stromatolite buildups. Spatially, the northwestern sections (JB1817/18 and JB1820) are characterized by a higher proportion of microbialite compared to the other measured sections (fig. 10), which could reflect an overall more protected or shoreward setting. In contrast, the central section (JB1815) comprises the core of an individual stromatolite buildup which at the outcrop scale is ~300 m across and had up to ~35 m of synoptic relief (figs. 10, 11). The instances of intraclast rudstone in the southeastern sections (fig. 10) could represent proximal stromatolite reef talus, which in addition to the predominance of cross-stratified lithofacies and increased thickness of the Gametrail at these locations, could indicate a higher-energy, basinward position.

The Goz D carbonate lithofacies share similarities with other Neoproterozoic stromatolite and thrombolite patch

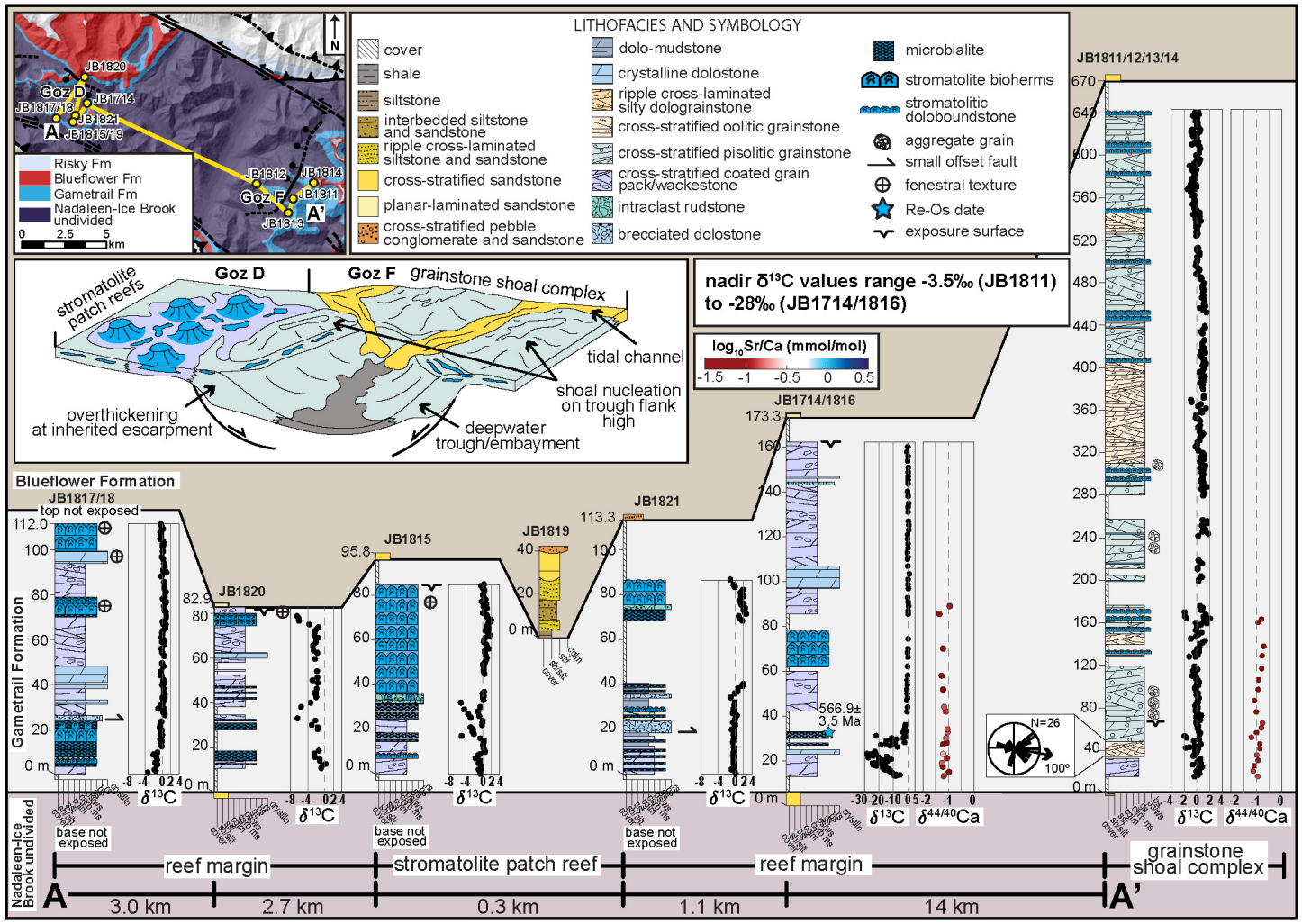

Figure 10. Detailed measured sections and carbon and calcium isotope stratigraphy of the Gametrail Fm for the southern Goz Creek region (Goz D-F block) of the Wernecke Mountains, Yukon. Inset map in the upper left depicts the location of each measured section, and below is a cartoon depositional model for this area (not to scale). Calcium isotope data is colored by the $\log_{10}$Sr/Ca ratios (mmol/mol). Note that the Goz F composite section has a different vertical scale than the other stratigraphic sections. Dip-corrected paleocurrent data from Goz F is plotted as a rose diagram (arrow indicates the mean vector). sh-shale; silt-siltstone; sst-sandstone; cglm-conglomerate; carb ms-carbonate mudstone; gs-grainstone; ps/ws-packstone/wackestone; bs-boundstone; rs-rudstone; crystlln-crystalline.

reef complexes described elsewhere. For example, in the Nama Group of Namibia, stromatolite patch reefs interfinger with peri-reef grainstone deposits in an outer ramp setting (Adams et al., 2005), while in the Wilpena Group of Australia, stromatolite patch reefs interfinger with shale in a similar outer ramp environment (Lemon, 2000). The stromatolite patch reef system described here in the Gametrail Fm has more indications of shallow-water sedimentation due to the abundant high-energy subtidal deposits and potential evidence for subaerial exposure at the upper contact with the Blueflower Fm (see below; fig. 10). Furthermore, the overall finer-grained reef margin lithofacies compared to the Nama Group could indicate an environment where the stromatolite buildups were large enough to sufficiently protect and sustain a lower-energy shoreward environment.

The upper contact with the Blueflower Fm is locally marked by bright maroon staining associated with coarse-grained ferruginous carbonate cements and breccias, which may reflect evidence for *terra rossa* development formed during subaerial exposure and karstification (for example, Merino & Banerjee, 2008). However, it is unclear if the >35 m of synoptic relief between the base of the Blueflower Fm clastics and the top of the Gametrail Fm stromatolitic buildups is a result of erosional beveling or simple filling of empty accommodation space during subsequent flooding (or some combination of the two). The lack of clear evidence for karst collapse features and/or fluvial erosion along the flanks of the buildups, along with the apparent onlap of generally fine-grained siliciclastic strata of the Blueflower Fm, suggests this transition may simply record abrupt cessation of the carbonate system by an increased flux of siliciclastic detritus.

3.2.3. Goz F: Description

The Goz F location is a new name designation for a region we investigated to the east of Goz D (figs. 2, 8), just west of measured sections published by Fritz et al. (1983) and the "Goz E" locality of Osborne et al. (1986). Measured sections of the Gametrail Fm at Goz F record another dramatic shift in thickness and carbonate lithofacies only 14 km southeast of Goz D (fig. 6). Here, the Gametrail Fm is exposed primarily as vertical cliff faces due to its relatively shallow dip (~15°; fig. 11E), precluding the measurement of a continuous stratigraphic section. Therefore, a composite section of the Gametrail Fm was pieced together from four overlapping stratigraphic sections measured within ~3.5 km of each other where the cliff exposures were navigable. The estimated total thickness of the Gametrail Fm is ~670 m and the basal contact with the undivided Nadaleen-Ice Brook formations is covered.

The Gametrail Fm commences with 17 m of medium-bedded trough cross-stratified coated grain packstone composed of spheroidal to ellipsoidal grains and sharing many similarities to facies observed at Goz D (FA6; figs. 10, 11F). Towards the top of this interval, these strata entirely consist of ripple- to dune-scale trough cross-stratified oolitic dolograinstone with bimodal paleocurrents (FA6; fig. 10). Most of the overlying strata at Goz F are dominated by similar monotonous packages of medium- to thick-bedded oolitic to pisolitic (giant ooid) dolograinstone with amalgamated planar bedding and/or visible ripple- to dune-scale trough cross-stratification (FA6; figs. 10, 11G). Petrographic examination of the oolitic and pisolitic lithofacies indicate the matrix is predominantly anhedral dolomite spar, while the grain nuclei consist of fine-grained dolomite, dolomite spar, and subrounded fine- to medium-grained quartz sand. Preservation of radial cortices is exceptional in some grains, and others are rimmed by isopachous or fibrous cements (fig. 11G). A cryptic erosional surface with up to ~30 cm of relief that incises into underlying oolitic dolograinstone occurs at ~70 m and is filled by coarse-grained quartz sandstone (fig. 10). This erosional surface is directly overlain by a package of irregular to convolute bedding with brecciated clasts of dolograinstone, which is then overlain by a distinctive grapestone-bearing wackestone and packstone interval composed of granule- to gravel-sized aggregate grains filled with pisoids and ooids (figs. 10, 11F). Rare intervals of stromatolitic doloboundstone (FA3) do appear infrequently throughout the Gametrail Fm at Goz F, which are characterized by hemispheroidal (2–20 cm in diameter) and domal (0.5–1 m in diameter) morphologies and local ferruginous carbonate cements (fig. 10). The upper contact with the Blueflower Fm is marked by an abrupt covered interval with poorly exposed siltstone and black shale, while the lowest exposed beds of the overlying Blueflower Fm consist of trough cross-stratified medium-grained sublitharenite interbedded with siltstone (FA11-13; fig. 10).

3.2.4. Goz F: Interpretation

A shallow subtidal or intertidal interpretation for the Gametrail Fm at Goz F is supported by the ubiquitous occurrence of trough cross-stratified coarse-grained carbonate lithofacies that indicate consistent sedimentation above fair-weather wave base. Overall, these strata resemble prominent ooid or coated grain shelf margin or interior shoal complexes, where most of the carbonate sediment is being consistently reworked by strong wave and/or storm action (for example, Rankey & Reeder, 2011; Read, 1985; Trower et al., 2018). The rare occurrence of stromatolitic doloboundstone within the predominantly coarse-grained carbonate lithofacies may be similar to other Proterozoic–Modern carbonate successions where stromatolites occur in laterally adjacent protected subtidal or supratidal settings (for example, Dill, 1991; Hoffman, 1974; Read, 1985). The presence of grainstone with abundant quartz sand matrix and quartz sand-dominated coated grain cortices may suggest that tidal distributary channels funneled siliciclastic material into this predominantly subtidal to intertidal setting (fig. 10); however, the lack of abundant channel morphologies or thick sandstone-dominated intervals suggest an eolian source may also be possible.

The broader depositional context of the Gametrail Fm in the Goz F region is challenging due to the remarkable thickness and apparent constancy of the recorded depositional setting. Shallow-water environments where most ooids and aggregate grains are produced commonly lack the accommodation space necessary to preserve an overthickened shoal complex without significant base level rise and/

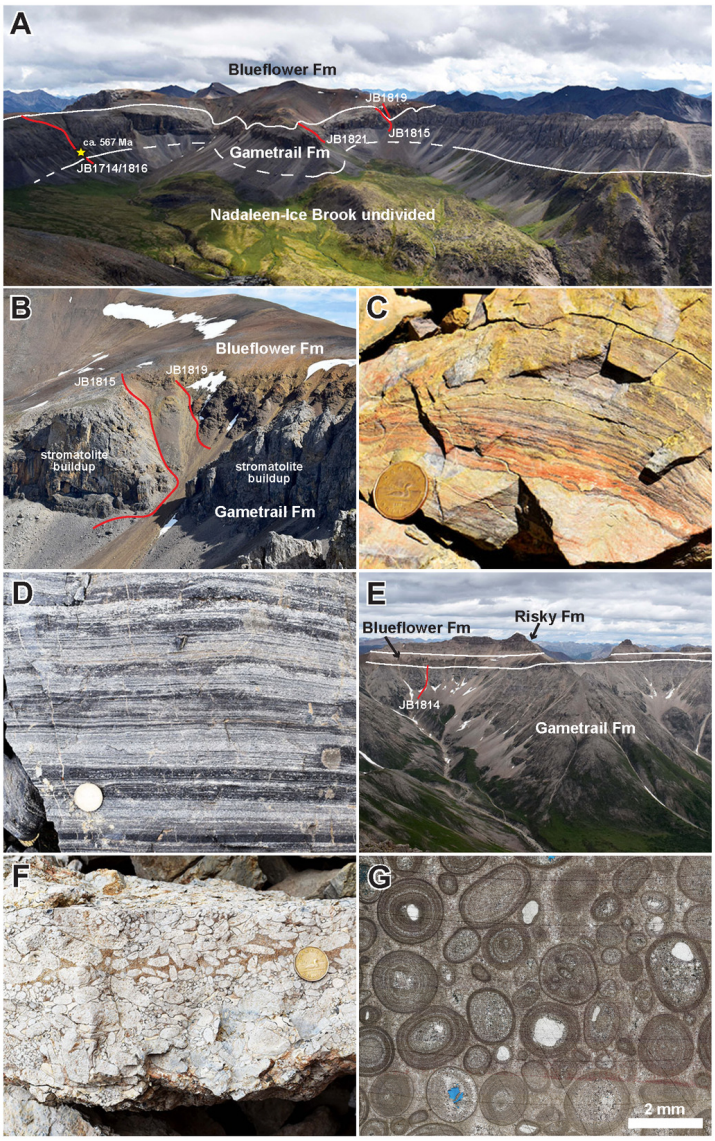

Figure 11. Photo panel of field relationships and representative lithofacies from the Gametrail Fm in the Goz D-F block. Red lines indicate measured sections plotted in fig. 10. (A) Image looking southeast at one of the primary exposures of the Gametrail Fm in the Goz D panel. Yellow star indicates sampling location for Re-Os date shown in figs. 10 and 12. (B) Two adjacent stromatolite patch reefs with siliciclastic fill of the Blueflower Fm between them (brown-weathering rocks in the background). (C) Brightly colored ferruginous carbonate laminae in a domal stromatolite horizon (FA3) from section JB1815. Coin is 2.7 cm in diameter. (D) Interbedded microbialite (dark layers; FA4) and gently cross-stratified coated grain pack-/wackestone (lighter layers; FA5). Coin is 2.7 cm in diameter. (E) Image looking north at the Goz F location. Note thickness contrasts between the Blueflower and Gametrail formations compared to Goz D. (F) Granule- to cobble-sized grapestone aggregates composed of ooids and other coated grains in a fine- to medium-grained quartz sand matrix (FA6) at Goz F. Coin is 2.7 cm in diameter. (G) Plane-polarized light (PPL) photomicrograph of oolitic/pisolitic dolograinstone from the Goz F region (FA6). Note the radial cortices are visible in some grains and that several of the grain nuclei are subrounded quartz sand particles.

or tectonic subsidence. Deep intrashelf troughs can accommodate thick packages of redeposited oolitic grainstones, such as those observed in the Glen Rose Formation of the Houston trough (Soto-Kerans et al., 2021); however, the dearth of obvious interbedded suspension deposits and the abundance of wave-generated bedforms and common stromatolite occurrences argue against a deeper-water origin for the Gametrail Fm at Goz F. One possibility is that this region records a proximal foreslope debris tongue adjacent to an unidentified paleohigh or embayment (fig. 10; for example, Playton et al., 2010). A local paleohigh may have served as an important source of sediment production for an adjacent embayment where there was sufficient accommodation space to accumulate an overthickened package of grainstone. The importance of paleohighs and antecedent topography for the development of ooids shoals has been

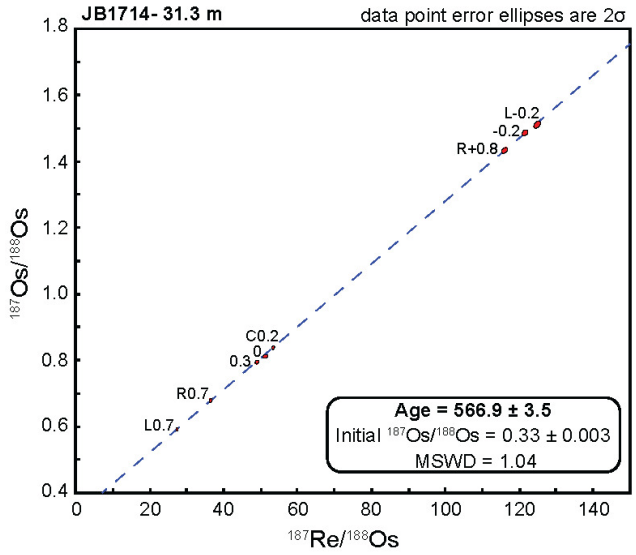

Figure 12. Re-Os isochron diagram for sample JB1714-31.3 m from the Gametrail Fm at Goz D (see figs. 8, 10, and 11 for location information). All isotopic composition and elemental abundance data are presented in Supplemental S4.

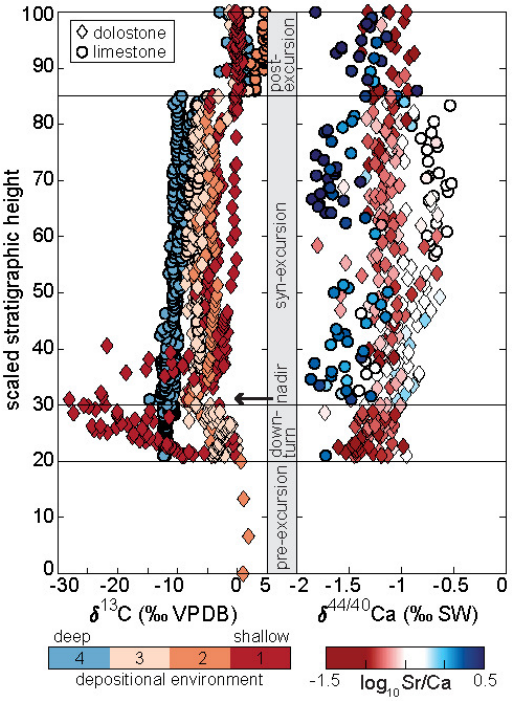

Figure 13. Summary stratigraphic plots of $\delta^{13}C$ and $\delta^{44/40}Ca$ data for the Gametrail Fm after Busch et al. (2022). Gradients in both carbon and calcium isotopes occur with water depth, where increasing water depth is generally associated with more negative $\delta^{44/40}Ca$ and $\delta^{13}C$ values, although the Goz D data is an exception to this trend (see text for discussion). Note that the most negative $\delta^{44/40}Ca$ values with the highest Sr/Ca are not obviously associated with the $\delta^{13}C$ nadir indicated by the black arrow.

extensively discussed for the Smackover and Buckner formations (Benson et al., 1996) and the thickest Bahamian ooid accumulations notably occur at the edge of deeper-water embayments (Hine et al., 1981).

4. Rhenium-Osmium (Re-Os) Geochronological Results

An organic-rich microbialite horizon from the lower part of the Gametrail Fm at Goz D was sampled for Re-Os geochronology (section JB1714, 31.3 m; figs. 10, 11A) and yielded a Model 1 depositional age of 566.9 ± 3.5 Ma (2σ, n = 6, MSWD = 1.04) with an initial $^{187}Os/^{188}Os$ (Os_i) composition of 0.33 ± 0.004 (fig. 12). The Re-Os date is stratigraphically near the return to 0‰ above a highly negative CIE that is described further below (fig. 10).

5. Geochemical Results

5.1. Northern Corn/Goz Creek – Nadaleen River shelf-slope transect

The basal part of the Gametrail Fm at Goz A and B contains positive $\delta^{13}C$ values up to +1.8‰ and preserves a sharp downturn to -4.5‰ (fig. 6). At Goz A, $\delta^{13}C$ profiles then reach a nadir of -8.5‰ with accompanying $\delta^{44/40}Ca$ data ranging -1.3 to -1.1‰ and generally low Sr/Ca. At Goz B, $\delta^{13}C$ profiles reach a nadir of -8.1‰ and $\delta^{44/40}Ca$ measurements range from -1.4 to -1.2‰ with higher Sr/Ca values. The base of the Goz C section begins with negative $\delta^{13}C$ values of -3.7‰ and $\delta^{44/40}Ca$ of -1.5‰, which both gradually increase to ~ -1‰ at ~90 m with consistently low Sr/Ca (fig. 6). In contrast to other sections, a nadir of -7‰ at Goz C occurs much higher in the section and is associated with higher $\delta^{44/40}Ca$ values up to -1‰ and slightly elevated Sr/Ca (fig 6). All three Nadaleen River measured sections have $\delta^{13}C$ nadirs that occur close to the base of the Gametrail Fm (ranging from -14.7 to -12.6‰), with more negative $\delta^{44/40}Ca$ values (ranging from -1.9 to -1.3‰) and high Sr/Ca (fig. 6).

At all locations with complete sections of the Gametrail Fm along the shelf-slope transect, $\delta^{13}C$ values above the nadir gradually trend towards 0‰ before a rapid shift to positive values (figs. 6, 13). Where there is $\delta^{44/40}Ca$ data across this transition at Goz A and C, there is a subtle but statistically significant shift (mean values (μ): μ_{S2} = -1.2‰, μ_{S1} = -1.1‰, $p < 0.01$) to more positive values with low Sr/Ca (fig. 6). At the SE Rackla location, the shift to more positive $\delta^{13}C$ and $\delta^{44/40}Ca$ is of a larger magnitude compared to the northern Corn/Goz Creek sections, with $\delta^{13}C$ values reaching +2.2‰ and $\delta^{44/40}Ca$ reaching -0.9‰ with a decrease in Sr/Ca (fig. 6). The Nadaleen Mountain and NW Rackla sections do not record the uppermost portion of the Gametrail Fm. At Goz A and C, $\delta^{13}C$ values are consistently more positive (ranging from -1.8 to +0.9‰) in the upper part of the sections, while $\delta^{44/40}Ca$ values are also consistently more positive (ranging -1.4 to -0.9‰; fig. 6). However, at SE Rackla the $\delta^{44/40}Ca$ profile returns to more negative values of ~ -1.5‰, while $\delta^{13}C$ values reach a peak of +2.2‰ before declining to -3‰ at the contact with the Blueflower Fm (fig. 6).

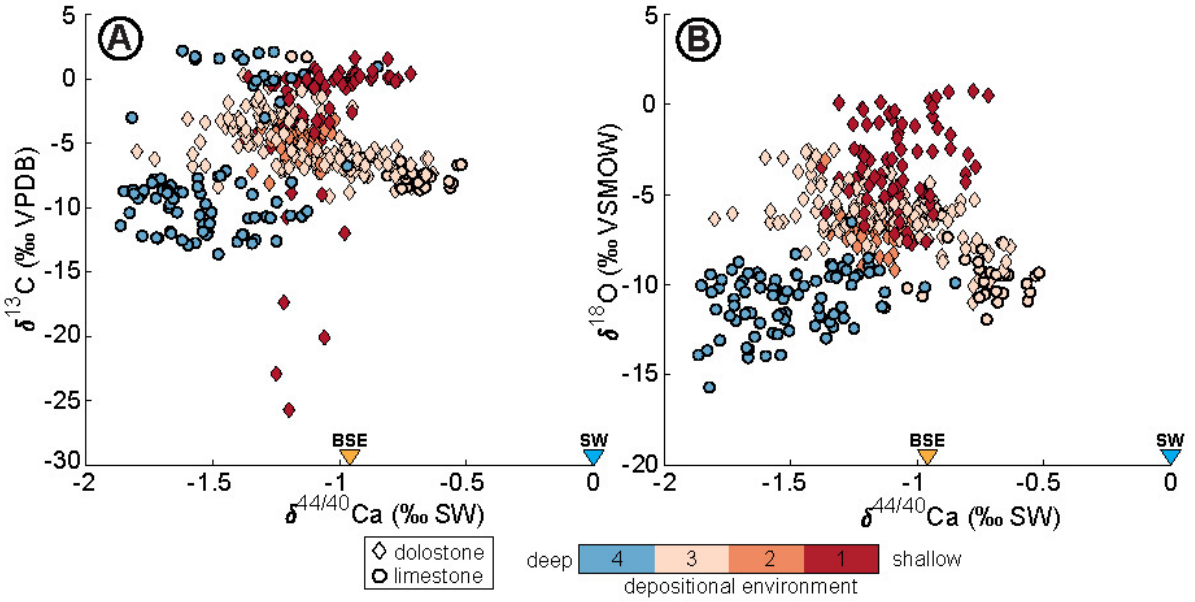

Figure 14. Cross-plots of (A) $\delta^{13}C$ vs. $\delta^{44/40}Ca$ and (B) $\delta^{18}O$ vs. $\delta^{44/40}Ca$ from the Gametrail Fm. Sample symbology indicates bulk mineralogy (limestone vs. dolostone) and color represents relative water depth by depositional environment. BSE = bulk silicate Earth (-0.96‰; Skulan et al., 1997); SW = seawater (0‰). Depositional environment color coding is as follows: 1 = inner ramp/reef complex/shoal complex (Goz A/D/F), 2 = middle ramp (Goz B and Coal Creek inlier; Busch et al., 2022), 3 = outer ramp (Goz C), 4 = slope (NW Rackla, Nadaleen Mtn, SE Rackla).

$\delta^{18}O$ data generally covary with $\delta^{13}C$ in both the Corn/Goz Creek and Nadaleen River regions (fig. 14). At Goz A-C, the most negative $\delta^{18}O$ values (~ -9‰) occur with the $\delta^{13}C$ nadir and gradually increase to ~0‰ at Goz A and ~ -6‰ at Goz B-C towards the top of the Gametrail Fm. In the Nadaleen River area, the most negative $\delta^{18}O$ values (~ -14‰) also occur with the $\delta^{13}C$ nadir and gradually increase to ~ -8‰ towards the top of the Gametrail Fm. Like $\delta^{13}C$, there is a strong positive covariation between $\delta^{18}O$ and $\delta^{44/40}Ca$ (fig. 14), where more negative $\delta^{18}O$ values from the Nadaleen River area limestones are associated with the most negative $\delta^{44/40}Ca$ values, and the Corn/Goz Creek dolostones have more positive $\delta^{44/40}Ca$ and $\delta^{18}O$ values.

5.2. Goz D-F block

The measured sections from the Goz D-F block contain significant variation in $\delta^{13}C$ between adjacent sections (fig. 10); however, it should be noted that only one measured section from Goz D (JB1714/1816) traverses the entire unit, including the recessive lower interval with highly negative $\delta^{13}C$ data that is covered at all the other locations.

At Goz D, the only similarity between the $\delta^{13}C$ profiles is a predominance of values close to ~0‰, especially in the upper part of the Gametrail Fm (fig. 10). Sections JB1820, JB1815, and JB1821 all have $\delta^{13}C$ profiles that begin at ~0‰, while JB1714/1816 and JB1817/18 begin with negative values ranging from -8.9 to -3.5‰. JB1820 and JB1815 both contain intervals of negative $\delta^{13}C$ values down to -6.4 and -5.2‰, respectively, while JB1714/1816 records a sharp decrease in $\delta^{13}C$ values to -28‰. In contrast, JB1817/18 and JB1821 do not record any negative $\delta^{13}C$ values below -3.5‰. Most sections record an interval of more positive $\delta^{13}C$ values ranging from -1.1 to +2.6‰ in the upper part of the Gametrail Fm, with JB1820 as the notable exception where $\delta^{13}C$ values remain negative throughout the section before reaching values of -6.5‰ at the contact with the Blueflower Fm. Only one section (JB1714/1816) from Goz D also has accompanying $\delta^{44/40}Ca$ and trace element data, and the profile does not contain any observable trend or significant difference before and after the $\delta^{13}C$ excursion, with values ranging from -1.4 to -1‰ with low Sr/Ca (fig. 10). Overall, $\delta^{18}O$ profiles from the Goz D sections display significant variation and contain values ranging from -8 to 0‰. Unlike most other locations along the transect, the most negative $\delta^{18}O$ values observed in the Goz D profiles do not occur with the $\delta^{13}C$ nadir and overall do not covary with the $\delta^{13}C$ data (fig. 14).

The Goz F $\delta^{13}C$ profile contains no highly negative values like other Gametrail sections. The composite section begins with $\delta^{13}C$ values of -0.3‰ and reaches a minimum nadir of -1.9‰ at 53 m (fig. 10). The only coherent trend in the profile is a gradual increase to maximum positive $\delta^{13}C$ values of +2.1‰ at 164 m, followed by a gradual decrease to 0.3‰ at the contact with the Blueflower Fm. The $\delta^{44/40}Ca$ profile also does not display any observable trend, with values ranging from -1.2 to -0.7‰ and accompanying

low Sr/Ca (fig. 10). $\delta^{18}O$ values range between ~ -8 and 0‰ and have more point-to-point variation by comparison with other localities; however, unlike Goz D, the $\delta^{18}O$ data do positively covary with the $\delta^{13}C$ and $\delta^{44/40}Ca$ data.

6. Sequence Stratigraphy of the Gametrail Formation

Building upon previous work by MacNaughton et al. (2000), Pyle et al. (2004), and Macdonald et al. (2013) for the Rackla Group more broadly, we apply a transgressive-regressive (T-R) sequence stratigraphic approach (Embry, 2009) to interpret the sequence stratigraphy of the Gametrail Fm in the Wernecke Mountains. Following the T-R framework, we define subaerial unconformities and their correlative conformities as the boundary between successive depositional sequences. The Gametrail Fm contains two to three distinct T-R sequences in most locations (labeled S1, S2, and S3 in fig. 15), albeit with significant differences between the northern Corn/Goz Creek and Nadaleen River regions (fig. 15A) and the Goz D-F block (fig. 15B). Given the complexity of the observed stratigraphic relationships, these preliminary interpretations will need to be further integrated with future observations from the bracketing Nadaleen and Blueflower formations.

Within the Corn/Goz Creek-Nadaleen River shelf-slope transect, the base of the first T-R sequence (S1) is marked by a subaerial exposure surface at Goz A-B and an inferred disconformity between shallow marine siliciclastic rocks of the Nadaleen Fm and overlying carbonate strata of the Gametrail Fm at Goz C (fig. 15A). The correlation of this T-R sequence into deeper water deposits of the Nadaleen River area is not straightforward given the lack of an equivalent subaerial exposure surface. In the Corn/Goz Creek region, the S1 T-R sequence is characterized by positive $\delta^{13}C$ values, in contrast to the overlying S2 sequence which bears highly negative $\delta^{13}C$ values (fig. 6). In contrast, the basal carbonates of the Gametrail Fm in the Nadaleen River region commence with highly negative $\delta^{13}C$ values (figs. 6, 15A). The underlying upper carbonate member of the Nadaleen Fm in the Nadaleen River region records positive $\delta^{13}C$ values (Moynihan et al., 2019) and could reflect a distal equivalent to this S1 sequence. However, the presence of a 574.0 ± 4.7 Ma Re-Os depositional age in the Nadaleen Fm unambiguously beneath this sequence at Goz A and an overlapping Re-Os date of 575.0 ± 5.1 Ma from the lower black shale member of the Nadaleen Fm in the Nadaleen River area (Rooney et al., 2020) suggests the deep-water expression of the S1 sequence is either absent, condensed, or equivalent to coarse-grained siliciclastic rocks preserved in the upper black shale and green siliciclastic members of the Nadaleen Fm (figs. 4D, 15A; Moynihan et al., 2019).

While the base of the S2 sequence is a prominent erosional surface at Goz A-B and covered at Goz C (Fig. 6), it is most likely a correlative conformity at the base of the Gametrail Fm in the Nadaleen River area (fig. 15A). This is supported by highly negative $\delta^{13}C$ values of the nadir of the Shuram CIE that characterize this sequence. The upper boundary of the S2 T-R sequence is marked by a subaerial exposure surface and paleokarst interval at Goz A-B and the abrupt appearance of siliciclastic strata at Goz C (figs. 6, 15A). In the Nadaleen River region, this boundary is likely marked by an abrupt but conformable shift to more siliciclastic-rich carbonate in the upper part of the Gametrail Fm (figs. 4C, 6).

In the Corn/Goz Creek region, the S3 T-R sequence is characterized by a poorly exposed, siliciclastic-dominated transgressive phase and a carbonate-dominated regressive phase whose top marks the Gametrail-Blueflower contact (figs. 6, 15A). The upper boundary of the S3 T-R sequence at all these sites is marked by a subaerial exposure surface separating vuggy and/or fenestral crystalline dolostone from siliciclastic rocks of the Blueflower Fm. The S1 and S3 T-R sequences are notably thinner by comparison with the S2 sequence, and both are also characterized by positive $\delta^{13}C$ values. In the Nadaleen River region, the upper S3 sequence boundary is represented by a correlative conformity from carbonate- to siliciclastic-dominated lithologies at the Gametrail-Blueflower contact (fig. 15A).

In the Goz D locality, the Gametrail Fm appears to only record a single T-R sequence (S2), while the Goz F region either contains one or two sequences (fig. 15B). This T-R sequence is tentatively correlated with the S2 sequence along the Corn/Goz–Nadaleen River shelf-slope transect because it contains highly negative $\delta^{13}C$ values and is overlain by another T-R sequence in the Blueflower Formation that may ultimately be equivalent to the S3 sequence (figs. 6, 10, 15B). At Goz D, the presumed lower S2 sequence boundary is represented by a disconformity between basal carbonate strata of the Gametrail Fm and underlying siliciclastic rocks of the undivided Nadaleen-Ice Brook formations, while the potential subaerial surface at the top of the Gametrail Fm represents the upper S2 sequence boundary (fig. 15B). The proposed S3 sequence in the overlying Blueflower Fm at Goz D contains mixed siliciclastic-carbonate rocks with an upper sequence boundary marked by a prominent subaerial exposure surface within a prominent sandy oolitic dolograinstone marker unit in the upper part of the Blueflower Fm (boundary of yuletide and disk members of Pyle et al., 2004). It is also possible that the Gametrail Fm at Goz D could all be part of sequence S3; however, because there is a large negative CIE correlated with the Shuram CIE at the base of the carbonate succession at Goz D (fig. 10), we retain the current division between the Gametrail and Blueflower formations as occurring at the S2-S3 sequence boundary (fig. 15B).

In the Goz F locality, the basal sequence boundary is represented by a disconformity between carbonate of the Gametrail Fm and underlying siliciclastic rocks of the undivided Nadaleen/Ice Brook formations (fig. 15B). The cryptic sequence boundary at ~70 m in the measured section, locally marked by an irregular erosional surface and quartz sandstone interval, could reflect a boundary between two T-R sequences; however, this surface could also reflect spatial heterogeneity in the depositional environment at Goz F since it did form a prominent marker bed throughout the region (see depositional model in fig. 10). The top of the Gametrail Fm is marked by a prominent disconformity with siliciclastic rocks of the Blueflower Fm. In contrast to all

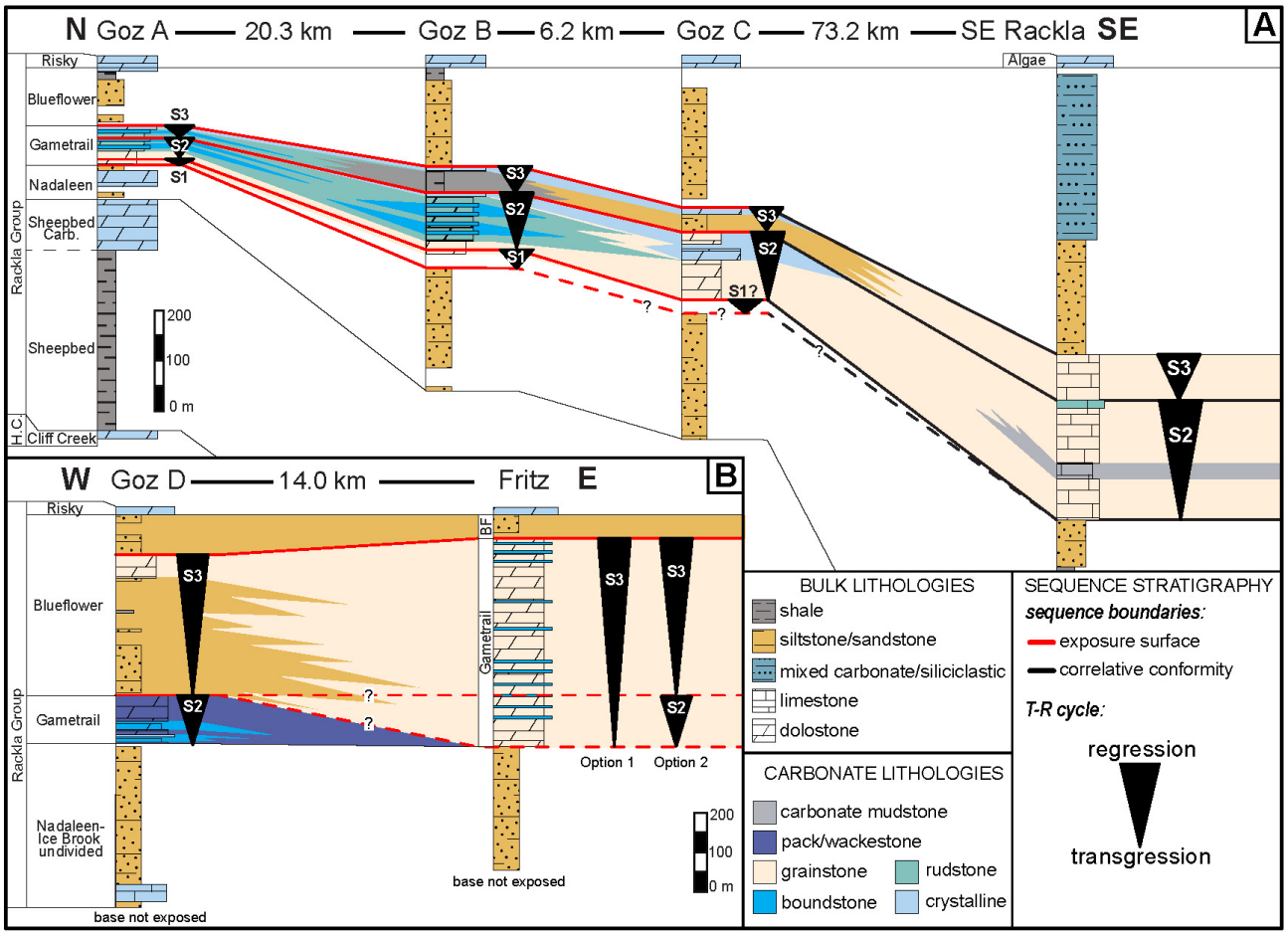

Figure 15. Gametrail Fm transgressive-regressive (T-R) sequence stratigraphic interpretations from this study modified after Boag (2020), Macdonald et al. (2013), and Pyle et al. (2004). Coloring of lithofacies between sections is interpretive and intended to be schematic. See text for a detailed discussion of correlations between T-R sequences. (A) Sequence stratigraphy for the northern Corn/Goz Creek – Nadaleen River shelf-slope transect with three depositional sequences (S1-S3) separated by subaerial exposure surfaces. These surfaces mark the sequence boundaries at Goz A-C and generally transition into correlative conformities in the deeper water Nadaleen River region. Note that the lower S1 sequence is interpreted to be present in the lower covered interval at Goz C, although it is possible that it is absent. (B) Sequence stratigraphic interpretations for the Goz D-F structural panel. Note how most, if not all, of the Gametrail Fm at Goz F is interpreted to be correlative with the Blueflower Fm at Goz D and the remainder of the Goz A-C panel. H.C.-Hay Creek; Carb.-Carbonate; BF-Blueflower.

other locations in the Wernecke Mountains, the T-R sequence(s) at Goz F do not contain highly negative $\delta^{13}C$ values (< -3‰), and instead record consistent values around 0‰ (fig. 10). Given these relationships, we suggest the Goz F locality either records a single S3 sequence or a poorly developed expression of the S2 and S3 sequences (fig. 15B).

7. Discussion

7.1. Regional Correlations and Origins of the Goz D-F Block

We suggest the prominent siliciclastic unit underlying the Gametrail Fm in both the Goz A-C transect and the Goz D-F block is correlative with the Nadaleen Fm of Moynihan et al. (2019). Although there are currently no identified lithofacies of the Sheepbed and/or Cliff Creek formations beneath this siliciclastic unit in the Goz D-F block (fig. 15), the correlation of these strata with the Nadaleen Fm is supported by a couple lines of evidence. First, the siltstone-dominated lithofacies of the sub-Gametrail strata at Goz D and F are similar to those described from the Nadaleen Fm at Goz B and C, although the unit is much thicker by comparison (Boag, 2020). Second, the disconformity between carbonate lithofacies of the Gametrail Fm at Goz D and F and deeper-water siliciclastic lithofacies of the underlying unit is not obviously suggestive of a significant temporal hiatus (fig. 11A, E). It is important to note, however, that Pyle et al. (2004) described channelized sandstone units directly beneath carbonate strata of the Gametrail Formation at Goz D (their peritidal carbonate member of the Blueflower Formation), so an important erosional surface may exist beneath the Gametrail Formation on the Goz D-

F block. In addition, there is another example in the Wernecke Mountains where the Gametrail Fm may sit unconformably on early Ediacaran units (Ambrose, 2022), so it is possible the sub-Gametrail Fm unit on the Goz D-F block correlates to an older unit, such as the Ice Brook Formation. As a result of these ambiguities, we have kept this unit undivided on our current map (figs. 3, 8), but we stress the importance of clarifying these relationships in future work given the aforementioned complexities of litho-, chrono-, and sequence stratigraphic correlations within the Goz D-F block, as well as other regions in the Mackenzie Mountains (e.g., Sekwi Brook; Macdonald et al., 2013).

As highlighted previously, the Gametrail Fm was first imported from the Mackenzie Mountains to the Corn/Goz Creek region of the Wernecke Mountains by Aitken (1989) to what was previously lumped into the unnamed siltstone 2 of Fritz et al. (1983) and siltstone unit 2 of Aitken (1984), and then upgraded to a separate "Sheepbed carbonate" unit by Narbonne et al. (1985) (table 1). These correlations were subsequently revised by Pyle et al. (2004) and Macdonald et al. (2013) and then extended to the Nadaleen River region by Moynihan (2014) and Moynihan et al. (2019) (table 1) and the Ogilvie Mountains by Macdonald et al. (2013) and Busch et al. (2021). In the Ogilvie Mountains, the Gametrail Fm is correlative with the recently formalized Last Chance Fm, where it sits above black shale of the Mount Ina Fm and below siltstone of the Shade Fm (fig. 2; Busch et al., 2021).

Based on our study, we also propose a slight revision to the definition of the Gametrail Fm in the Nadaleen River area to encompass all carbonate strata immediately above the Nadaleen Fm, including the more siliciclastic-rich upper succession (sequence S3 of fig. 15) that was formerly assigned to the "lower carbonate member" of the basal Blueflower Fm by Moynihan et al. (2019) (table 1). Our reasoning is that from a mapping perspective, the Gametrail Fm is much more clearly defined as a prominent mid-Ediacaran carbonate-dominated unit bracketed by two early-middle Ediacaran siliciclastic-dominated units.

The extraordinary thickness of the Gametrail Fm in the Goz F region (~4x thicker than Goz D) paired with the marked thinning of the Blueflower Fm (~7.5x thinner than Goz D) means that a simple correlation of carbonate sequences in the Gametrail Fm between Goz D and F, and then beyond to the Goz/Corn Creek or Nadaleen River regions, is unrealistic when considering the accommodation space available below the Risky Fm, a widespread regional marker unit. Therefore, it is hypothesized here that much, if not all, of the Gametrail Fm at Goz F is chronostratigraphically equivalent to the Blueflower Fm at Goz D (fig. 15B). This is supported by the short distance between locations (~14 km) and the presence of oolitic dolograinstone lithofacies in the upper Blueflower Fm at Goz D that are identical to those at Goz F. In addition, it is also notable that there are no highly negative $\delta^{13}C$ values in the Gametrail Fm at Goz F, which are typically diagnostic of the lower S2 depositional sequence elsewhere in the Wernecke Mountains (figs. 6, 10).

Recognition of the overlying Lower Cambrian Sekwi Fm in the Goz D-F block suggests that ~30 km of Mesozoic–Cenozoic dextral strike-slip displacement across a major fault strand of the Snake River transcurrent fault system could restore the Goz D-F block to equivalent exposures of the Sekwi Fm further to the southeast (figs. 3, 8). This displacement would remove the Goz D-F block from its current centralized geographic position in the shelf-slope transect between the Corn/Goz Creek and Nadaleen river areas and help alleviate challenging internal stratigraphic correlations within the Gametrail Fm across the transect as a whole. Assuming this restoration is reasonable, prior to the Cordilleran orogeny, the Goz D-F block would have been situated adjacent to the "Snake River Basin" where early Cryogenian extension and/or transtension influenced deposition of the Rapitan and Hay Creek groups (Baldwin et al., 2016; Eisbacher, 1981; Macdonald et al., 2018) as well as the later Misty Creek Embayment (Cecile et al., 1982), an important early Paleozoic depocenter. This region is also part of the much larger Richardson Fault array, which not only forms the eastern boundary of the Yukon block, but also records a complex history of Neoproterozoic deformation and subsidence (Abbott, 1997; Cecile et al., 1982; Eisbacher, 1981; Strauss et al., 2015); thus, the recognition of anomalous subsidence patterns in the Ediacaran succession of the Goz D-F block (fig. 10) would be consistent when considering its restored geographic position (fig. 8).

Correlations between the type section of the Gametrail Fm at Sekwi Brook in the Mackenzie Mountains and other regions in NWT and Yukon are complicated by inconsistent chemostratigraphic data, abrupt lateral changes in unit thicknesses, and a paucity of radiometric age constraints on Ediacaran strata more broadly (Macdonald et al., 2013; MacNaughton et al., 2008; Moynihan et al., 2019; Okulitch & Irwin, 2016). For example, the Gametrail Fm at Sekwi Brook yields $\delta^{13}C$ data that do not contain highly negative values characteristic of the Shuram CIE elsewhere (maximum negative values of ~ -2‰; Macdonald et al., 2013), thereby complicating a simple chemostratigraphic correlation with the Gametrail Fm in the Wernecke Mountains and the Last Chance Fm of the Ogilvie Mountains (Busch et al., 2021; Moynihan et al., 2019).

It was observed during a 2011 traverse at Sekwi Brook, as well as in recent mapping compilations (Okulitch & Irwin, 2016), that the Gametrail Fm pinches out laterally along strike in the type area. This lateral discontinuity could be the result of synsedimentary truncation due to slope failure, or alternatively, it could represent the lateral pinching out of Gametrail Fm slope channel fill. In either scenario, it is currently ambiguous whether the type Gametrail Fm at Sekwi Brook is correlative with the entire Gametrail Fm preserved elsewhere in northwestern Canada. For example, it is possible that only the upper part of the Gametrail Fm is preserved at Sekwi Brook (that is, only correlative with sequence S3 from the Wernecke Mountains), or alternatively, the type Gametrail Fm strata could be correlative with the siliciclastic-dominated lower Blueflower Fm preserved elsewhere, similar to what is discussed above for the Gametrail Fm in the Goz F section. Alternatively, it is possible that carbonate strata of the Gametrail Fm at Sekwi Brook are indeed correlative to the Shuram CIE-bearing Gametrail Fm

in the Wernecke Mountains but have since been isotopically reset during fluid-buffered diagenesis. Regardless of the potential correlations of the Gametrail Fm, we propose that the carbonate-dominated succession of the lower Blueflower Fm at Sekwi Brook should be included with the Gametrail Fm moving forward, similar to what we propose for the Gametrail and Blueflower formations in the Nadaleen River area. This would simplify regional lithostratigraphic correlations for these units, while acknowledging the complexity of direct chronostratigraphic correlations throughout the upper Ediacaran succession of northwestern Canada.

Ediacaran fossil impressions characteristic of the *ca.* 570 Ma Avalon assemblage have been described from the Nadaleen Fm at Sekwi Brook, including the hold-fast discs *Aspidella* and fronds such as *Charniodiscus*, *Charnia*, *Beothukis*, and *Primocandelabrum* (Narbonne et al., 2014). The upper Blueflower Fm contains both simple Ediacaran trace fossils (Carbone & Narbonne, 2014) and body fossils, including *Aspidella*, a possible dickinsoniid *Windermeria*, and tubular body fossils such as *Sekwitubulus* and *Annulatubus* (Carbone et al., 2015; Hofmann, 1981; Narbonne, 1994; Narbonne et al., 2014; Narbonne & Aitken, 1990) that are characteristic of the terminal Ediacaran (*ca.* 550–540 Ma) Nama Assemblage (Schiffbauer et al., 2016). These biostratigraphic constraints permit the Gametrail Fm at Sekwi Brook to be correlative with the post-Shuram CIE interval of the Avalon assemblage, or alternatively a pre-Blueflower Fm part of the White Sea or Nama assemblage (Boag, 2020). In summary, we suggest the sedimentological, geochemical, and biostratigraphic data suggest the Gametrail Fm at Sekwi Brook post-dates the nadir of the Shuram CIE and is correlative with the uppermost sequence of the Gametrail Fm in the Wernecke Mountains (sequence S3) and the Fireweed member of the Last Chance Fm in the Ogilvie Mountains (fig. 2).

7.2. Stratigraphic evolution of the Gametrail Formation in the Wernecke Mountains, Yukon

The Gametrail Fm of the Wernecke Mountains chronicles the evolution of a complex distally steepened carbonate ramp in response to changes in base level and tectonic subsidence alongside unique global changes to the isotopic composition of marine carbonate rocks (Busch et al., 2022). Deposition of the Gametrail Fm commenced <575 Ma (Rooney et al., 2020) with the thin to absent T-R sequence S1 that is poorly preserved in the proximal Corn/Goz Creek locations (Goz A/B) and provides little information about the nature of the depositional system during the nascent development of the carbonate margin. However, the lower depositional sequence does have indications of subtidal to peritidal sedimentation above shallow-water siliciclastic and carbonate rocks of the Nadaleen Fm and includes negative $\delta^{13}C$ values from the downturn of the Shuram CIE (figs. 6, 16A). In the distal Nadaleen River region, this lower sequence is either condensed, absent, or reflected as an ~150 m thick interval of coarse-grained siliciclastic strata in the uppermost Nadaleen Fm (upper black shale and green siliciclastic members).

Subsequent base level fall led to subaerial exposure and erosion of an unknown thickness of the lower sequence, but it was followed by a prominent transgression (base of T-R S2) that flooded all locations, establishing Goz C in an outer ramp and Goz A-B within inner to middle ramp positions (fig. 16B). In the more distal Nadaleen River region, this transgression is recorded by the first appearance of carbonate above the upper siliciclastic members of the Nadaleen Fm (figs. 6, 15, 16B). At all locations, this flooding is coincident with the downturn (where present) and nadir of the Shuram CIE. The proximal carbonate depositional system during the S2 sequence is characterized by inner-middle ramp facies dominated by cross-stratified grainstone, stromatolitic boundstone, and storm-generated deposits (fig. 16B). In contrast, the outer ramp is dominated by fine-grained grainstone with less persistent influence by storm-generated wave currents. On the slope, the S2 depositional sequence is predominantly composed of turbiditic mudstone and silty limestone with occasional debris flow deposits.

Subsequent regression led to subaerial exposure, karstification, and local erosion of the uppermost S2 depositional sequence in the northern Corn/Goz Creek regions and potential removal of the entire S2 depositional sequence in the Goz F region (figs. 6, 10, 16C). In the distal Nadaleen River region, this regression is manifest in a distinct change to more siliciclastic-rich carbonate strata, perhaps reflective of enhanced transport of siliciclastic material onto the slope during the lowstand. At all locations, the S2-S3 sequence boundary is coincident with the termination of the Shuram CIE (S3; fig. 6, 15). At Goz A-C, the thin S3 depositional sequence is characterized by mixed siliciclastic-carbonate lithofacies with textures indicative of subtidal to peritidal sedimentation, perhaps reflecting progradation of shallower environments onto the outer ramp before it eventually became emergent. This upper S3 sequence boundary marks the unconformable contact with the Blueflower Fm in the proximal Goz Creek locations (fig. 16D). The more siliciclastic-rich S3 sequence in the distal Nadaleen River region contains evidence of deposition in a slope environment that is consistent with the underlying sequences, so evidently the drop in relative sea level at the S2-S3 boundary was not large enough to place the Nadaleen River area above the upper slope (fig. 6, 16).

Anomalous subsidence patterns in the Goz D-F block, potentially associated with proximity to an active Neoproterozoic fault system and associated intraplatformal trough, resulted in the development of a complex depositional system during Gametrail sedimentation (fig. 10, 16). A lack of accommodation space, either due to a position on a paleo-high or active uplift and erosion along the flank of the nascent trough, could explain the hypothesized condensed expression of the Shuram CIE at Goz D. This is consistent with both the predominance of positive $\delta^{13}C$ values in this block and our new 566.9 ± 3.5 Ma Re-Os date from the base of the Gametrail Fm in this location (fig. 12), suggesting the bulk of the unit's thickness postdates the nadir of the Shuram CIE (fig. 10). The thickness and facies changes across the Goz D-F block and its relationship to

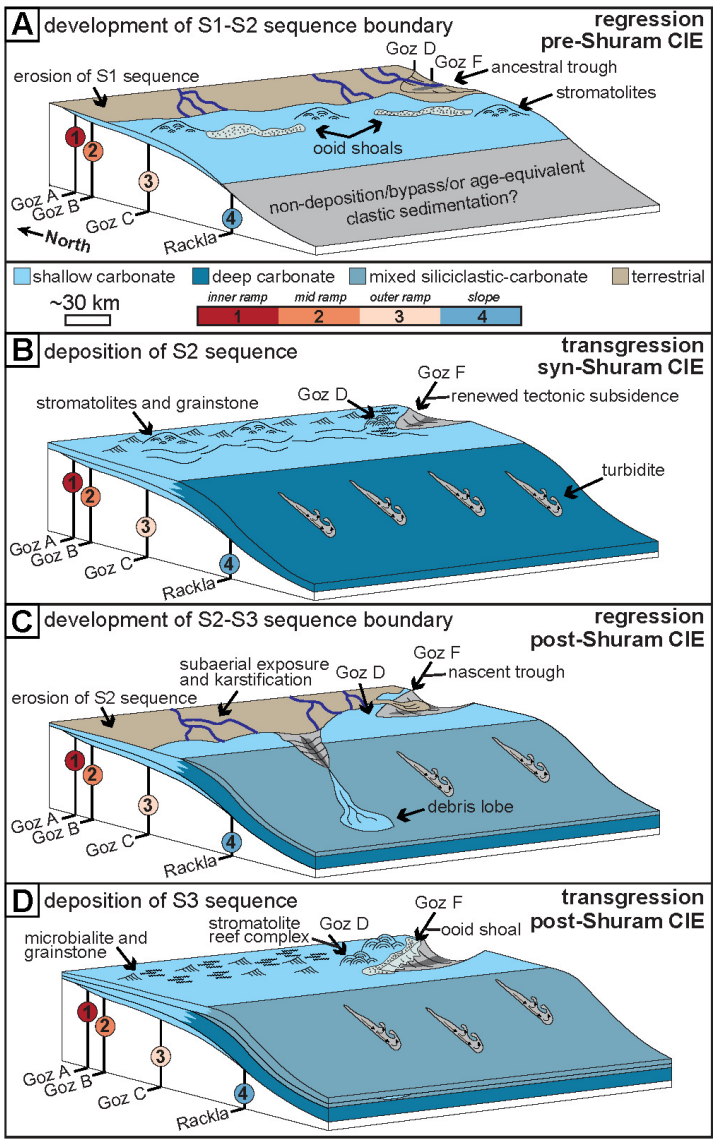

Figure 16. Schematic depositional model for the stratigraphic evolution of the Gametrail Fm in the Wernecke Mountains. Note that the extent of depositional environments beyond our limited study area is extrapolated for the rest of the hypothetical margin. (A) Following deposition of the basal carbonate sequence (S1) in the Gametrail Fm inner-outer ramp, a regression leads to subaerial exposure and erosion on the shelf. An ancestral trough is interpreted to have influenced sedimentation in the Goz D-F block, and the sedimentation on the slope is either condensed, missing, or manifest in a succesion of clastic rocks in the upper black shale and green siliciclastic members of the Nadaleen Fm. (B) Transgression accompanies deposition of the thickest depositional sequence (S2) and floods inner-outer ramp environments. Stromatolite reef system develops adjacent to an ancestral trough on the Goz D-F block. (C) Regression leads to paleokarst development and erosion of the S2 sequence in inner-outer ramp environments, while mixed siliciclastic-carbonate material is delivered to the slope environment. Subsidence in the Goz D-F block prevents the developing stromatolite buildups from being subaerially exposed at the same stratigraphic interval as the Goz A-C sites. (D) Transgression leads to the deposition of the uppermost sequence (S3) and accompanies the establishment of the Goz D stromatolite patch reefs and ooid shoal complex on the flank of an ancestral trough.

the remarkably thick Goz F section likely indicates some influence of tectonic subsidence on the development of the carbonate system (e.g., localized development of the stromatolite reef buildup and coated grain shoal complex) and the local expression of the Shuram CIE (fig. 16). Coincident with deposition of the grainstone shoal complex at Goz F, a mixed siliciclastic-carbonate system developed in the more proximal Corn/Goz Creek regions (Goz A-D) and eventually prograded over Goz F marking the cessation of Gametrail carbonate sedimentation.

7.3. Geochemical trends in the Gametrail Formation

All the geochemical proxies have significant positive or negative correlations with interpreted depositional environment and mineralogy ($p < 0.01$; figs. 14, 17), suggesting a prominent water-depth gradient for multiple geochemical proxies through the Shuram CIE. However, it is important to consider how carbonate diagenesis has influenced the proxies among the disparate environments sampled here, especially given the different susceptibilities of isotope systems (for example, $\delta^{13}C$ vs. $\delta^{18}O$) to resetting during neomorphism, dissolution and reprecipitation, or dolomitization (for example, Ahm et al., 2018; Husson, Higgins, et al., 2015). Diagenetic studies of modern and ancient carbonate rocks using $\delta^{44/40}Ca$ and $\delta^{26}Mg$ isotopes, geochemical modeling, and trace element ratios have shown that carbonate diagenesis can be characterized as being buffered with respect to the surrounding rock (sediment-buffered) or seawater (fluid-buffered) (Ahm et al., 2018; Higgins et al., 2018). Sediment- and fluid-buffered end-members are distinguishable because calcium isotope fractionation and trace element partitioning between the fluid and rock are a function of mineralogy and precipitation rate (DeCarlo et al., 2015; Gussone et al., 2005). Primary aragonite and calcite have more negative $\delta^{44/40}Ca$ values and are enriched in metals such as Sr and U relative to diagenetic calcite and dolomite; these diagenetic phases have lower Sr and U concentrations and more positive $\delta^{44/40}Ca$ values that approach pore fluid compositions (Fantle & DePaolo, 2007).

In general, slope limestones from the Nadaleen River region contain more negative $\delta^{44/40}Ca$, high Sr/Ca and U/Ca, and low Mn/Sr suggestive that they have undergone sediment-buffered neomorphism from aragonite to calcite (fig. 14). In contrast, the inner-outer ramp dolostones of the Corn/Goz Creek area have more positive $\delta^{44/40}Ca$, low Sr/Ca and U/Ca, and high Mn/Sr indicative of fluid-buffered diagenesis during dolomitization. Overall, these trends are consistent with both modern data from the Bahamas Banks (fig. 14; Higgins et al., 2018) and other locations around the world that record the Shuram CIE (Busch et al., 2022). Given this diagenetic context, the more negative $\delta^{13}C$ values in slope limestones can be interpreted as being closer to their primary compositions, that is, the composition when initially precipitated from seawater, while the smaller $\delta^{13}C$ excursion in inner-outer ramp dolostones could reflect fluid-buffered alteration towards modern (and presumed post-Shuram CIE) seawater values, which are ~0‰ in $\delta^{13}C$. For the $\delta^{18}O$ data, it is more challenging to disentangle the influence of sediment-buffered diagenesis on the more negative $\delta^{18}O$ values recorded from the slope limestones due to the relatively high sensitivity of the oxygen isotopic system to resetting during diagenesis (Ahm et al., 2018; Husson, Maloof, et al., 2015). Indeed, there is an even stronger negative correlation between water depth and $\delta^{18}O$ ($r = -0.86$) compared to $\delta^{13}C$ ($r = -0.68$) reflecting this well-documented phenomenon (figs. 13, 14). However, it has been observed by others (for example, Derry, 2010) that primary $\delta^{18}O$ values as negative as those observed in the Gametrail slope limestones imply unrealistically hot seawater temperatures, which are probably more consistent with a burial diagenetic signature.

The Goz D-F block sections deviate significantly from the general geochemical trends observed along the shelf-slope transect. The $\delta^{13}C$ values from Goz D are more negative than any other location (down to ~ -30‰), show significant variation between adjacent sections, and are found within shallow water dolostones with $\delta^{44/40}Ca$, Sr/Ca, and Mn/Sr values consistent with fluid-buffered diagenesis (figs. 10, 13, 14). If interpreted in a similar diagenetic framework to the other locations described above, the highly negative $\delta^{13}C$ values at Goz D represent a fluid-buffered end-member that initially had more negative $\delta^{13}C$ values that were altered towards seawater values of ~0‰ during dolomitization. This is opposite of the trend observed from other locations along the shelf-slope transect, where more negative $\delta^{13}C$ values in the Shuram CIE are associated with slope environments due to the better preservation potential in deeper water. The prospect of initial $\delta^{13}C$ values even more negative than their current nadir of ~ -30‰ is problematic, and along with the significant variability in $\delta^{13}C$ between the different sections at Goz D, suggests a more nuanced explanation for the origin of the presumed Shuram CIE at this location. The new *ca.* 567 Ma Re-Os date at Goz D is from the return to ~0‰ at the end of the CIE (figs. 10, 12), which overlaps with the *ca.* 567 Ma date from the end of the Shuram CIE recorded elsewhere in northwestern Canada and globally (Rooney et al., 2020). However, because there are no age constraints in the upper Nadaleen Fm or lower in the Gametrail Fm beneath this horizon at Goz D, we cannot say unequivocally if deposition of the extremely isotopically depleted lower part of the Gametrail Fm at Goz D (~30 m thick) occurred over the same *ca.* 6-7 million-year (Myr) duration of the Shuram CIE.

Goz F is unique among all locations considered in this study in that it does not contain highly negative $\delta^{13}C$ values (minimum of ~ -2‰) characteristic of the Gametrail and Last Chance formations throughout Yukon. However, the absence of the Shuram CIE at Goz F is similar to the Gametrail Fm type section at Sekwi Brook (Macdonald et al., 2013). There are at least two broad possibilities for this relationship at Goz F: 1) either these carbonate strata postdate the Shuram CIE due to a depositional/erosional hiatus (as discussed above), or 2) they did record the Shuram CIE but were diagenetically reset during fluid-buffered diagenesis. If the Shuram CIE is interpreted as a global perturbation to the marine reservoirs of C and Ca isotopes over a timescale greater than the residence times for these elements, mass balance must be achieved through coeval deposition of more positive sinks to counter the highly negative values which characterize the excursion for both isotopic systems (Ahm et al., 2021; Busch et al., 2022). Thus, the more positive $\delta^{13}C$ and $\delta^{44/40}Ca$ values recorded at Goz F (figs. 6, 10) may represent an example of the positive sink which allows isotopic mass balance to be achieved during the apparent *ca.* 6–7 Myr duration of the Shuram CIE (similar to what has been discussed for the Trezona CIE by Ahm et al., 2021). In fact, it has been proposed

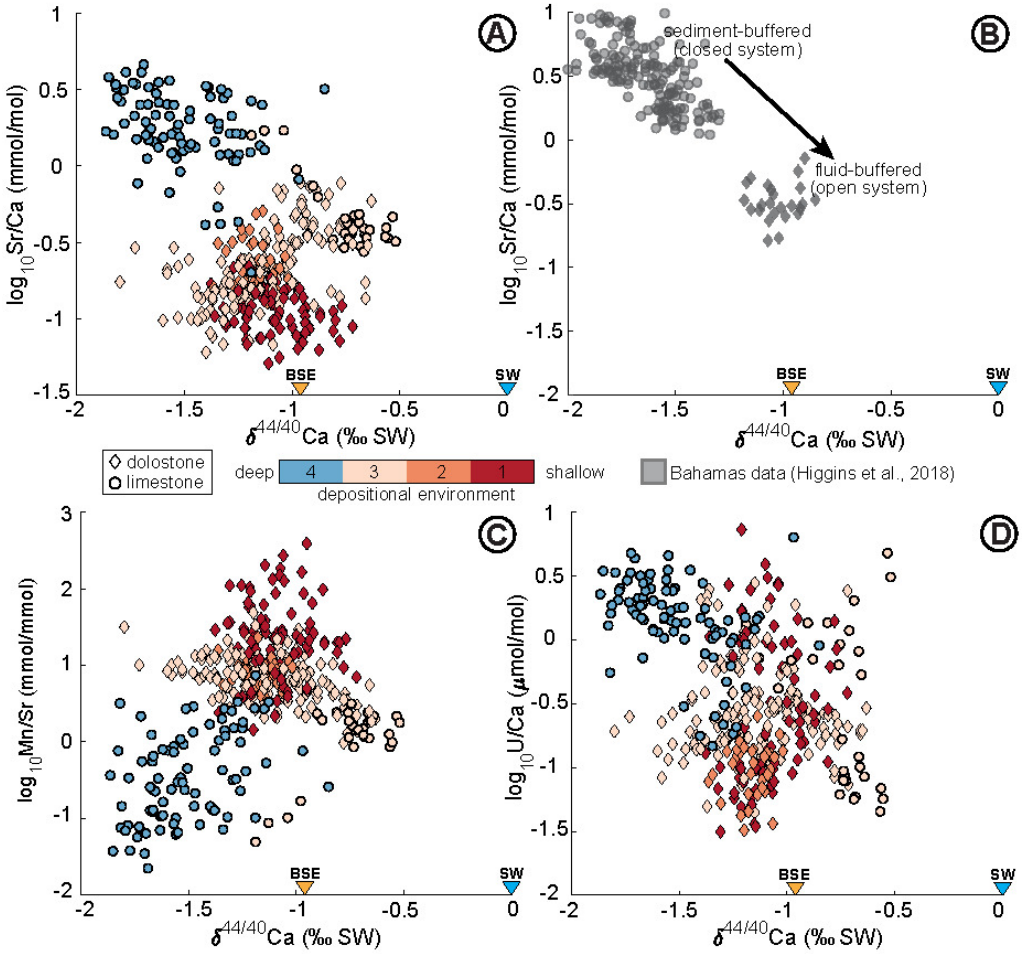

Figure 17. Cross-plots of geochemical data from the Gametrail Fm. Sample symbology indicates bulk mineralogy (limestone vs. dolostone) and color represents relative water depth by depositional environment. (A) log_{10}Sr/Ca vs. $\delta^{44/40}$Ca, (B) log_{10}Sr/Ca vs. $\delta^{44/40}$Ca for Bahamas data (Higgins et al., 2018), (C) log_{10}Mn/Sr vs. $\delta^{44/40}$Ca, (D) U/Ca vs. $\delta^{44/40}$*Ca*. BSE = bulk silicate Earth (-0.96‰; Skulan et al., 1997); SW = seawater (0‰). Depositional environment color coding is as follows: 1 = inner ramp/reef complex/shoal complex (Goz A/D/F), 2 = middle ramp (Goz B and Coal Creek inlier; Busch et al., 2022), 3 = outer ramp (Goz C), 4 = slope (NW Rackla, Nadaleen Mtn, SE Rackla).

in shallow shelf-edge environments (similar to those described from Goz F) that fluid-buffered diagenesis of carbonate rocks with open marine waters might be the best record of global $\delta^{13}C_{DIC}$ through time due to isotopic resetting with seawater representative of global marine DIC (Hoffman & Lamothe, 2019). However, it is noteworthy that other locations examined in this study that have clear evidence for fluid-buffered diagenesis (that is, Goz A-B) still bear negative $\delta^{13}C$ values characteristic of the Shuram CIE. Moreover, at Goz A-B there is direct evidence for the development of paleokarst and associated meteoric diagenesis at the upper contact of the Shuram-bearing S2 depositional sequence, which evidently was unable to diagenetically reset the underlying fluid-buffered dolostones beyond their current $\delta^{13}C$ values of ~ -6‰ (figs. 6, 7C). Therefore, it seems more likely that the Gametrail Fm at Goz F postdates the Shuram CIE rather than representing an example of total diagenetic resetting of Shuram-bearing carbonate rocks, especially given the complicated subsidence history for the region (see discussion above). If this interpretation is correct, it is a fantastic example of the complexities inherent in lithostratigraphic, chemostratigraphic, and chronostratigraphic correlations in Precambrian strata across even a well-characterized bathymetric transect.

7.4. Implications for the global Shuram Carbon Isotope Excursion (CIE)

The chemostratigraphic data from the Gametrail Fm in the Wernecke Mountains have important implications for understanding the origin and expression of the Shuram CIE globally. Similar to other locations on different paleocontinents, the Shuram CIE of Yukon and NWT occurs during a large transgression, and the magnitude of the excursion is largest in slope limestone deposits and smallest in inner-outer ramp dolostone strata (Busch et al., 2022). However, there are some key differences from the common global signal that may provide further insight into the variable expression of the Shuram CIE and perhaps other enigmatic Neoproterozoic $\delta^{13}C$ perturbations. In particular, the ab-

sence of the CIE at Goz F and the anomalously negative $\delta^{13}C$ values at Goz D may represent instructive examples for how local isotope reservoir effects or complications in the local subsidence/sedimentation history of carbonate margins can result in deviations from the global expression of Neoproterozoic CIEs. Possibilities for these anomalous expressions of the Shuram CIE observed on the Goz D-F block could include cyptic depositional hiatuses, precipitation of authigenic carbonate, isolated sub-basin isotope reservoir effects, and/or oxidation of methane.

Palinspastic restoration of the Goz D-F block to a location further removed from the Corn/Goz Creek-Nadaleen River shelf-slope transect underscores the importance of interpreting the regional geology, map relationships, and structural history of a region before attempting to reconstruct its depositional environments or make litho- and chronostratigraphic correlations. Indeed, it is possible that cryptic stratigraphic hiatuses and/or other complexities that are sometimes difficult to recognize in the field could explain locations where globally recognized CIEs are unexpectedly absent or have markedly different expressions. For instance, recent radiometric dates from the Doushantuo Fm of South China led to the confirmation of a late Ediacaran (*ca.* 550 Ma) CIE that is distinct from the Shuram CIE and apparently has only been recently recognized in several successions around the world (Yang et al., 2021). The absence of this late Ediacaran CIE from carbonate successions elsewhere globally might be a prime example of how common stratigraphic hiatuses related to eustasy or tectonism could result in limited regional expression of a major CIE, rather than the excursion simply representing a regional or local phenomenon.

The highly negative $\delta^{13}C$ values observed at the base of the Goz D stromatolite reef buildup are anomalous in all other Shuram-CIE bearing locations in northwestern Canada and most locations around the world, but they bear a striking resemblance to those described from the Doushantuo Fm in South China. In the outer shelf region of the Doushantuo Fm, authigenic calcite nodules record $\delta^{13}C$ values down to ~ -30‰ and were interpreted to be the result of an episode of carbonate authigenesis in the sulfate–methane transition zone (Cui et al., 2017). Like the Wernecke Mountains, other locations in South China record typical expressions of the Shuram CIE, but the outer shelf region is a notable outlier in both the anomalously negative $\delta^{13}C$ values and their occurrence in multiple stratigraphic horizons (Cui et al., 2017). In contrast to the Shuram CIE in South China, however, the Goz D carbonates lack characteristic macroscopic authigenic textures, such as void-filling or porosity occluding cements, seafloor precipitates, and/or secondary nodules (fig. 18), which argues against authigenic carbonate precipitation during early diagenesis as a primary driver for the anomaly at this location.

Similarly negative $\delta^{13}C$ values (down to ~ -41‰) have also been observed in Marinoan cap carbonates of the Nantuo Fm in South China within ostensibly well-preserved primary carbonate textures and were interpreted to be related to oxidation of methane hydrates (Jiang et al., 2003). The oxidation of methane clathrates in seawater (Bjerrum

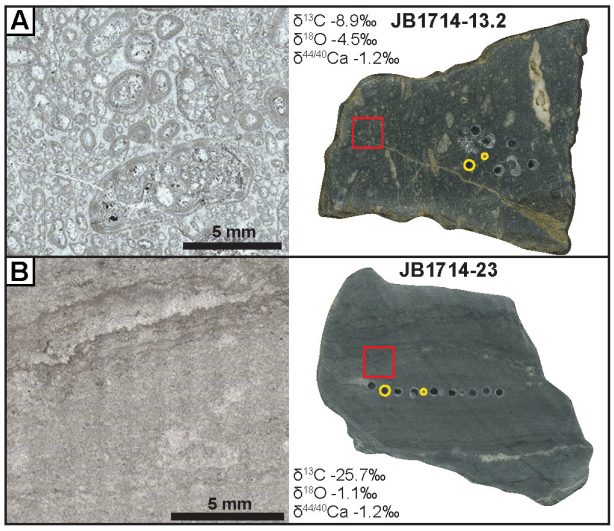

Figure 18. Plane-polarized light photomicrographs (shown on the left) and corresponding hand samples from the Gametrail Fm at Goz D. The areas shown in the thin sections are depicted on the right with red boxes, and sample drill holes for isotopic measurements are indicated by the yellow circles (with different diameters reflecting different drill bits). Multiple powders were drilled from different areas to test for isotopic reproducibility. (A) Coated grain dolopackstone from the lower Gametrail Fm at Goz D. Note the abundance of aggregate and individual coated grains composed of dark grey, fine-grained anhedral dolomite with porosity-occluding subhedral dolomite cement comprising the matrix. (B) Microbialite from the potential nadir interval of the Shuram CIE in the lower Gametrail Fm at Goz D. Note the fine-grained nature of the anhedral dolomite that composes the laminations, the presence of very-fine grained peloids and coated grains, and the lack of any obvious authigenic cements.

& Canfield, 2011; Jiang et al., 2003), as well as anoxic oxidation of methane produced by methanogenesis in sediment pore fluids (Cui et al., 2017) or the oxidation of methane, organic matter, or petroleum produced during thermal maturation of organic carbon during burial diagenesis (Derry, 2010), could all be viable explanations for anomalous magnitude of the Shuram CIE at Goz D. This is because the $\delta^{13}C_{CO2}$ of microbially oxidized methane is ~-30 to -40‰, while oxidized marine organic matter is ~ -20 to -30‰ (Barker & Fritz, 1981; Blättler et al., 2021; Sarmiento & Gruber, 2006). Importantly, however, it has been noted that the oxidant requirements for methane as a global driver for the Shuram CIE might exceed the oxidant pool for an oxygen-poor Ediacaran atmosphere (Grotzinger et al., 2011 and references therein), in addition to the large temporal mismatch between the relatively short residence time of methane in the atmosphere and oceans and the hypothesized *ca.* 6–7 Myr duration of the Shuram CIE (for example, Lamontagne et al., 1973; Prather, 1995). These oxidant and temporal considerations, however, might not be

relevant in a localized or potentially restricted setting such as the Goz D locality considered here, so they could easily explain this local phenomenon.

Spatial heterogeneity in $\delta^{13}C$ observed at other Shuram CIE localities has been explained through the oxidation of a pool of DOC through reaction with a variable supply of oxidants (that is, O_2 and sulfate) in marginal near-surface environments (Li et al., 2017). However, the hypothesized duration of the Shuram CIE requires that the mechanism for spatial heterogeneity in $\delta^{13}C$ be feasibly sustained over millions of years, which is difficult to achieve from an oceanographic perspective. Furthermore, and perhaps more importantly, there is no direct geochemical evidence for such a hypothesized pool of DOC, and there is no known mechanism by which DOC levels higher than modern levels can be sustained (Arrieta et al., 2015; Fakhraee et al., 2021).

It is also possible to drive solution DIC beyond mantle input values of ~ -5‰ through isotope reservoir effects (for example, Lazar & Erez, 1992), although the feasibility of this phenomenon is unclear in open marine settings. Photosynthetic drawdown of DIC can cause atmospheric CO_2 invasion and drive a significant carbon isotope fractionation (~ -14‰) during hydration reactions (Herczeg & Fairbanks, 1987; Lazar & Erez, 1992), a phenomenon which has been invoked for the Shuram CIE despite the inverse relationship between CO_2 invasion and carbonate saturation (Busch et al., 2022). Physical restriction of Goz D water masses, perhaps related to the local hydrology of the stromatolite reef complex, may have been capable of driving local DIC to these extreme values, similar to what has been observed in modern restricted settings (Lazar & Erez, 1992). However, it is unclear why the same mechanism invoked for other locations in northwestern Canada and around the world would result in such an anomalous difference in $\delta^{13}C$ values at Goz D. Moreover, there are plenty of other examples of Precambrian marine stromatolite buildups developed during episodes of carbon isotope volatility that lack these extremely negative $\delta^{13}C$ values (e.g., Halverson et al., 2007; Hoffman et al., 2012; Rose et al., 2012).

In summary, although the preponderance of geological evidence suggests a depositional hiatus is likely for the absence of the Shuram CIE at Goz F, a variety of explanations are still possible for the anomalously negative CIE observed at Goz D. Currently, it is difficult to unequivocally rule out some of these possibilities, and we suggest that further work using microanalytical techniques such as secondary ion mass spectrometry (for example, Cui et al., 2021; Husson et al., 2020) would help probe potential micron-scale variation in the isotopic composition of these unusual carbonates to better understand their origins.

8. Conclusions

In this study, we reconstructed the distribution of depositional environments for the Ediacaran Gametrail Fm along a shelf-slope transect in the Wernecke Mountains of Yukon, Canada, and identified paleowater depth gradients for multiple geochemical proxies in the globally recognized Shuram CIE. Overall, inner-outer ramp environments in the northern Corn/Goz Creek region are dominated by wave-influenced dolograinstone, stromatolitic dolobound-stone, and intraclast dolorudstone, while slope settings in the more distal Nadaleen River region are dominated by hemipelagic limestone mudstone, turbidites, and debris flows. The Goz D and F locations, which were previously considered a part of the Corn/Goz Creek depositional transect, are outliers with respect to their sedimentology, sequence stratigraphy, and geochemistry. Goz D is comprised of a complex stromatolite reef system with a single recognizable depositional sequence, while Goz F represents an overthickened coated grain shoal complex with either one or two depositional sequences. Regional map relationships and recognition of major Mesozoic–Cenozoic strike-slip faults bounding the Goz D-F block suggest that a more accurate palinspastic restoration places this crustal block ~30 km to the southeast adjacent to the Cryogenian Snake River Basin and early Paleozoic Misty Creek Embayment, which are locations of anomalous subsidence related to regional episodes of extension and/or transtension.

The Shuram CIE is expressed in the second of three depositional sequences identified in the Gametrail Fm along the shelf-slope transect and its magnitude is strongly correlated with interpreted water depth and mineralogy. Overall, the excursion is largest in slope limestone strata that underwent sediment-buffered diagenesis and more subdued in inner-outer ramp dolostone deposits that experienced fluid-buffered diagenesis. Again, the Goz D-F block is an outlier to this trend, with an anomalously large and condensed negative $\delta^{13}C$ excursion recorded in the lower Gametrail Fm at Goz D and no clear expression of the CIE at Goz F. Oxidation of methane and/or organic matter during early or burial diagenesis with subsequent precipitation of authigenic carbonate may explain the highly anomalous negative values; however, the lack of authigenic textures at Goz D confounds this interpretation, leaving open the possibility that physical restriction on the Goz D platform led to enhanced isotopic reservoir effects hypothesized as occurring globally in shallow marine environments during the Shuram CIE-associated transgression. In contrast, the absence of the Shuram CIE at the Goz F location is interpreted to potentially reflect deposition after the nadir of the Shuram CIE, similar to the Gametrail Fm at its type section in Sekwi Brook. This may have occurred due to a cryptic stratigraphic or erosional hiatus beneath the Gametrail Fm, but it is an important example of how local litho-, chemo-, and chronostratigraphic complications can explain the presence or absence of globally recognized CIE's in similarly aged carbonate units.

Acknowledgments

We are grateful to the Na-Cho Nyäk Dun and Tr'ondëk Hwëch'in First Nation communities for granting us permission to work in the Wernecke Mountains. This project was supported by: National Science Foundation (NSF) grants EAR-1654131 and EAR-2021176 awarded to JVS; National Geographic Society Grant EC-393R-18 awarded to JFB and

CP-102R-17 to EAS; American Philosophical Society Lewis and Clark grant awarded to JFB; and a Geological Society of America (GSA) graduate student research grant awarded to JFB. This project also received generous field support from the Geological Survey of Canada and the Yukon Geological Survey. We thank Joshua Landis, Stefania Gili, Jack Murphy, and Nic Slater for assistance in the lab and Max Saylor, Jack Taylor, Brenhin Keller, Akshay Mehra, and Emily Geyman for help in the field. Robert MacNaughton and Karen Fallas of the Geological Survey of Canada are thanked for their generous logistical support and fantastic insight into the regional geology of the Mackenzie Mountains. We thank Page Chamberlain and Tim Lyons for editorial handling of this manuscript. This contribution benefited from thoughtful reviews by Chao Li and an anonymous reviewer.

Author Contributions

JVS and EAS conceived the project and raised funding to support it, in addition to independent support garnered by JFB and THB. JFB, THB, EAS, DPM, and JVS performed fieldwork and collected samples. JFB, THB, ADR, and XF performed analytical work. JFB and JVS wrote an initial draft of the manuscript and all authors contributed to the final version.

SUPPLEMENTARY INFORMATION

https://earth.eps.yale.edu/~ajs/SupplementaryData/2023/Busch

Editor: C. Page Chamberlain, Associate Editor: Timothy W. Lyons

Submitted: June 09, 2022 EST, Accepted: April 14, 2023 EST

References

Abbott, G. (1997). Geology of the upper Hart River Area, eastern Ogilvie Mountains, Yukon Territory (116A/10, 116A/11. *Yukon Geology*, *9*.

Adams, E. W., Grotzinger, J. P., Watters, W. A., Schröder, S., McCormick, D. S., & Al-Siyabi, H. A. (2005). Digital characterization of thrombolite-stromatolite reef distribution in a carbonate ramp system (terminal Proterozoic, Nama Group, Namibia). *American Association of Petroleum Geologists Bulletin*, *89*(10), 1293–1318. https://doi.org/10.1306/06160505005

Ahm, A.-S. C., Bjerrum, C. J., Blättler, C. L., Swart, P. K., & Higgins, J. A. (2018). Quantifying early marine diagenesis in shallow-water carbonate sediments. *Geochimica et Cosmochimica Acta*, *236*, 140–159. https://doi.org/10.1016/j.gca.2018.02.042

Ahm, A.-S. C., Bjerrum, C. J., Hoffman, P. F., Macdonald, F. A., Maloof, A. C., Rose, C. V., Strauss, J. V., & Higgins, J. A. (2021). The Ca and Mg isotope record of the Cryogenian Trezona carbon isotope excursion. *Earth and Planetary Science Letters*, *568*, 117002. https://doi.org/10.1016/j.epsl.2021.117002

Aitken, J. D. (1966). *Sub-Fairholme Devonian rocks of the eastern Front Ranges, southern Rocky Mountains, Alberta* (Vol. 64). Geological Survey of Canada. https://doi.org/10.4095/101006

Aitken, J. D. (1978). Revised models for depositional grand cycles, Cambrian of the southern Rocky Mountains, Canada. *Bulletin of Canadian Petroleum Geology*, *26*, 515–542. https://doi.org/10.35767/gscpgbull.26.4.515

Aitken, J. D. (1984). *Strata and trace fossils near the Precambrian - Cambrian boundary, Mackenzie, Selwyn and Wernecke Mountains, Yukon and Northwest Territories: Discussion* (Current Research Part B Paper 84-1B; pp. 401–407). Geological Survey of Canada. https://doi.org/10.4095/119602

Aitken, J. D. (1989). *Uppermost Proterozoic formations in central Mackenzie Mountains, Northwest Territories*. Geological Survey of Canada. https://doi.org/10.4095/126611

Ambrose, T. (2022). Preliminary bedrock geology map of the Rusty Mountain and Bonnet Plume Pass areas, southern Wernecke Mountains, Yukon (NTS 106C/3, 4, 5, 6, 11, 12 and 106D/1, 8). Open File 2022-5. *Yukon Geological Survey*.

Arrieta, J. M., Mayol, E., Hansman, R. L., Herndl, G. J., Dittmar, T., & Duarte, C. M. (2015). Dilution limits dissolved organic carbon utilization in the deep ocean. *Science*, *348*(6232), 331–333. https://doi.org/10.1126/science.1258955

Badiozamani, K. (1973). The dorag dolomitization model, application to the middle Ordovician of Wisconsin. *Journal of Sedimentary Research*, *43*(4), 965–984. https://doi.org/10.1306/74d728c9-2b21-11d7-8648000102c1865d

Baldwin, G. J., Turner, E. C., & Kamber, B. S. (2016). Tectonic controls on distribution and stratigraphy of the Cryogenian Rapitan iron formation, northwestern Canada. *Precambrian Research*, *278*, 303–322. https://doi.org/10.1016/j.precamres.2016.03.014

Barker, J. F., & Fritz, P. (1981). Carbon isotope fractionation during microbial methane oxidation. *Nature*, *293*(5830), 289–291. https://doi.org/10.1038/293289a0

Benson, J. D., Pultz, L. M., & Bruner, D. D. (1996). The Influence of paleotopography, sea level fluctuation, and carbonate productivity on deposition of the Smackover and Buckner formations, Appleton Field, Escambia County, Alabama. *Transactions of the Gulf Coast Association of Geological Societies*, *46*, 15–23.

Beranek, L. P. (2017). A magma-poor rift model for the Cordilleran margin of western North America. *Geology*, *45*(12), 1115–1118. https://doi.org/10.1130/g39265.1

Bjerrum, C. J., & Canfield, D. E. (2011). Towards a quantitative understanding of the late Neoproterozoic carbon cycle. *Proceedings of the National Academy of Sciences*, *108*(14), 5542–5547. https://doi.org/10.1073/pnas.1101755108

Blättler, C. L., Hong, W.-L., Kirsimäe, K., Higgins, J. A., & Lepland, A. (2021). Small calcium isotope fractionation at slow precipitation rates in methane seep authigenic carbonates. *Geochimica et Cosmochimica Acta*, *298*, 227–239. https://doi.org/10.1016/j.gca.2021.01.001

Blättler, C. L., Miller, N. R., & Higgins, J. A. (2015). Mg and Ca isotope signatures of authigenic dolomite in siliceous deep-sea sediments. *Earth and Planetary Science Letters*, *419*, 32–42. https://doi.org/10.1016/j.epsl.2015.03.006

Blusson, S. L. (1974). *Five geological maps of northern Selwyn Basin (Operation Stewart), Yukon Territory and District of Mackenzie (105N, O; 106A, B, C). Open File 205*. Geological Survey of Canada. https://doi.org/10.4095/129320

Boag, T. H. (2020). *The role of ecophysiology and paleoenvironmental dynamics in the Ediacaran biostratigraphic record* [Ph.D thesis]. Stanford University.

Bouma, A. H. (1962). *Sedimentology of some flysch deposits: A graphical approach to facies classification*. Elsevier.

Burns, S. J., & Matter, A. (1993). Carbon isotopic record of the latest Proterozoic from Oman. *Eclogae Geologicae Helvetiae*, *86*(2), 595–607.

Busch, J. F., Hodgin, E. B., Ahm, A.-S. C., Husson, J. M., Macdonald, F. A., Bergmann, K. D., Higgins, J. A., & Strauss, J. V. (2022). Global and local drivers of the Ediacaran Shuram carbon isotope excursion. *Earth and Planetary Science Letters*, *579*, 117368. https://doi.org/10.1016/j.epsl.2022.117368

Busch, J. F., Rooney, A. D., Meyer, E. E., Town, C. F., Moynihan, D. P., & Strauss, J. V. (2021). Late Neoproterozoic – early Paleozoic basin evolution in the Coal Creek inlier of Yukon, Canada: Implications for the tectonic evolution of northwestern Laurentia. *Canadian Journal of Earth Sciences*, *58*(4), 355–377. https://doi.org/10.1139/cjes-2020-0132

Campbell, R. W., Beranek, L. P., Piercey, S. J., & Friedman, R. (2019). Early Paleozoic post-breakup magmatism along the Cordilleran margin of western North America: New zircon U-Pb age and whole-rock Nd- and Hf-isotope and lithogeochemical results from the Kechika Group, Yukon, Canada. *Geosphere*, *15*(4), 1262–1290. https://doi.org/10.1130/ges02044.1

Canfield, D. E., Knoll, A. H., Poulton, S. W., Narbonne, G. M., & Dunning, G. R. (2020). Carbon isotopes in clastic rocks and the Neoproterozoic carbon cycle. *American Journal of Science*, *320*(2), 97–124. https://doi.org/10.2475/02.2020.01

Carbone, C. A., & Narbonne, G. M. (2014). When life got smart: The evolution of behavioral complexity through the Ediacaran and early Cambrian of NW Canada. *Journal of Paleontology*, *88*(2), 309–330. https://doi.org/10.1666/13-066

Carbone, C. A., Narbonne, G. M., Macdonald, F. A., & Boag, T. H. (2015). New Ediacaran fossils from the uppermost Blueflower Formation, northwest Canada: Disentangling biostratigraphy and paleoecology. *Journal of Paleontology*, *89*(2), 281–291. https://doi.org/10.1017/jpa.2014.25

Cecile, M. P. (2000). *Geology of the northeastern Niddery Lake map area, east-central Yukon and adjacent Northwest Territories*. Geological Survey of Canada. https://doi.org/10.4095/211664

Cecile, M. P., Fritz, W. H., Norford, B. S., & Tipnis, R. S. (1982). *The Lower Paleozoic Misty Creek Embayment, Selwyn Basin, Yukon and Northwest Territories*. Geological Survey of Canada. https://doi.org/10.4095/111346

Colpron, M., Moynihan, D. P., Israel, S., & Abbott, G. (2013). *Geological map of the Rackla belt, east-central Yukon (NTS 106C/1-4, 106D/1). Open File 2013-13*. Yukon Geological Survey.

Colpron, Maurice, Logan, J. M., & Mortensen, J. K. (2002). U-Pb zircon age constraint for late Neoproterozoic rifting and initiation of the lower Paleozoic passive margin of western Laurentia. *Canadian Journal of Earth Sciences*, *39*(2), 133–143. https://doi.org/10.1139/e01-069

Cui, H., Kaufman, A. J., Xiao, S., Zhou, C., & Liu, X.-M. (2017). Was the Ediacaran Shuram Excursion a globally synchronized early diagenetic event? Insights from methane-derived authigenic carbonates in the uppermost Doushantuo Formation, South China. *Chemical Geology*, *450*, 59–80. https://doi.org/10.1016/j.chemgeo.2016.12.010

Cui, H., Kitajima, K., Orland, I. J., Xiao, S., Baele, J.-M., Kaufman, A. J., Denny, A., Zhou, C., Spicuzza, M. J., Fournelle, J. H., & Valley, J. W. (2021). Deposition or diagenesis? Probing the Ediacaran Shuram excursion in South China by SIMS. *Global and Planetary Change*, *206*, 103591. https://doi.org/10.1016/j.gloplacha.2021.103591

DeCarlo, T. M., Gaetani, G. A., Holcomb, M., & Cohen, A. L. (2015). Experimental determination of factors controlling U/Ca of aragonite precipitated from seawater: Implications for interpreting coral skeleton. *Geochimica et Cosmochimica Acta*, *162*, 151–165. https://doi.org/10.1016/j.gca.2015.04.016

Derry, L. A. (2010). A burial diagenesis origin for the Ediacaran Shuram–Wonoka carbon isotope anomaly. *Earth and Planetary Science Letters*, *294*(1–2), 152–162. https://doi.org/10.1016/j.epsl.2010.03.022

Diaz, M. R., & Eberli, G. P. (2019). Decoding the mechanism of formation in marine ooids: A review. *Earth-Science Reviews*, *190*, 536–556. https://doi.org/10.1016/j.earscirev.2018.12.016

Dill, R. F. (1991). Subtidal stromatolites, ooids, and crusted lime muds at the Great Bahama Bank margin. In R. H. Osborne (Ed.), *From Shoreline to Abyss:Contributions in Marine Geology in Honor of Francis Parker Shepard (Special Publication)* (Vol. 46, pp. 147–171). Society of Economic Paleontologists and Mineralogists (Society for Sedimentary Geology.

Eisbacher, G. H. (1981). *Sedimentary tectonics and glacial record in the Windermere Supergroup, Mackenzie Mountains, northwestern Canada*. Geological Survey of Canada. https://doi.org/10.4095/119453

Embry, A. F. (2009). Practical sequence stratigraphy. *Canadian Society of Petroleum Geologists*, *81*.

Eyster, A. E., Fu, R. R., Strauss, J. V., Weiss, B. P., Roots, C. F., Halverson, G. P., Evans, D. A. D., & Macdonald, F. A. (2016). Paleomagnetic evidence for a large rotation of the Yukon block relative to Laurentia: Implications for a low-latitude Sturtian glaciation and the breakup of Rodinia. *Geological Society of America Bulletin*, *129*(1–2), 38–58. https://doi.org/10.1130/b31425.1

Fakhraee, M., Tarhan, L. G., Planavsky, N. J., & Reinhard, C. T. (2021). A largely invariant marine dissolved organic carbon reservoir across Earth's history. *Proceedings of the National Academy of Sciences*, *118*(40), 2103511118. https://doi.org/10.1073/pnas.2103511118

Fantle, M. S., & DePaolo, D. J. (2007). Ca isotopes in carbonate sediment and pore fluid from ODP Site 807A: The Ca2+(aq)–calcite equilibrium fractionation factor and calcite recrystallization rates in Pleistocene sediments. *Geochimica et Cosmochimica Acta*, *71*(10), 2524–2546. https://doi.org/10.1016/j.gca.2007.03.006

Fike, D. A., Grotzinger, J. P., Pratt, L. M., & Summons, R. E. (2006). Oxidation of the Ediacaran Ocean. *Nature*, *444*(7120), 744–747. https://doi.org/10.1038/nature05345

Fritz, W. H., Narbonne, G. M., & Gordey, S. P. (1983). *Strata and Trace Fossils near the Precambrian-Cambrian Boundary, Mackenzie, Selwyn and Wernecke Mountains, Yukon and Northwest Territories* (Current Research Part B 83–1B; pp. 365–375). Geological Survey of Canada. https://doi.org/10.4095/109342

Gabrielse, H., Blusson, S. L., & Roddick, J. A. (1973). *Geology of Flat River, Glacier Lake, and Wrigley Lake map areas, District of Mackenzie and Yukon Territory*. Geological Survey of Canada.

Gibson, T. M., Faehnrich, K., Busch, J. F., McClelland, W. C., Schmitz, M. D., & Strauss, J. V. (2021). A detrital zircon test of large-scale terrane displacement along the Arctic margin of North America. *Geology*, *49*(5), 545–550. https://doi.org/10.1130/g48336.1

Grotzinger, J. P., Fike, D. A., & Fischer, W. W. (2011). Enigmatic origin of the largest-known carbon isotope excursion in Earth's history. *Nature Geoscience*, *4*(5), 285–292. https://doi.org/10.1038/ngeo1138

Gussone, N., Böhm, F., Eisenhauer, A., Dietzel, M., Heuser, A., Teichert, B. M. A., Reitner, J., Wörheide, G., & Dullo, W.-C. (2005). Calcium isotope fractionation in calcite and aragonite. *Geochimica et Cosmochimica Acta*, *69*(18), 4485–4494. https://doi.org/10.1016/j.gca.2005.06.003

Halverson, G. P., Hoffman, P. F., Schrag, D. P., Maloof, A. C., & Rice, A. H. N. (2005). Toward a Neoproterozoic composite carbon-isotope record. *Geological Society of America Bulletin*, *117*(9), 1181. https://doi.org/10.1130/b25630.1

Halverson, G. P., Maloof, A. C., Schrag, D. P., Dudás, F. Ö., & Hurtgen, M. (2007). Stratigraphy and geochemistry of a ca 800 Ma negative carbon isotope interval in northeastern Svalbard. *Chemical Geology*, *237*(1–2), 5–27. https://doi.org/10.1016/j.chemgeo.2006.06.013

Herczeg, A. L., & Fairbanks, R. G. (1987). Anomalous carbon isotope fractionation between atmospheric CO2 and dissolved inorganic carbon induced by intense photosynthesis. *Geochimica et Cosmochimica Acta*, *51*(4), 895–899. https://doi.org/10.1016/0016-7037(87)90102-5

Higgins, J. A., Blättler, C. L., Lundstrom, E. A., Santiago-Ramos, D. P., Akhtar, A. A., Crüger Ahm, A.-S., Bialik, O., Holmden, C., Bradbury, H., Murray, S. T., & Swart, P. K. (2018). Mineralogy, early marine diagenesis, and the chemistry of shallow-water carbonate sediments. *Geochimica et Cosmochimica Acta*, *220*, 512–534. https://doi.org/10.1016/j.gca.2017.09.046

Hine, A. C., Wilber, R. J., & Neumann, A. C. (1981). Carbonate sand bodies along contrasting shallow bank margins facing open seaways in northern Bahamas. *American Association of Petroleum Geologists Bulletin*, *65*(2), 261–290. https://doi.org/10.1306/2f9197ba-16ce-11d7-8645000102c1865d

Hoffman, P. F. (1974). Shallow and deepwater stromatolites in lower Proterozoic platform–to–basin facies change, Great Slave Lake, Canada. *American Association of Petroleum Geologists Bulletin*, *58*(5), 856–867. https://doi.org/10.1306/83d914a7-16c7-11d7-8645000102c1865d

Hoffman, P. F., Halverson, G. P., Domack, E. W., Maloof, A. C., Swanson-Hysell, N. L., & Cox, G. M. (2012). Cryogenian glaciations on the southern tropical paleomargin of Laurentia (NE Svalbard and East Greenland), and a primary origin for the upper Russøya (Islay) carbon isotope excursion. *Precambrian Research*, *206–207*, 137–158. https://doi.org/10.1016/j.precamres.2012.02.018

Hoffman, P. F., & Lamothe, K. G. (2019). Seawater-buffered diagenesis, destruction of carbon isotope excursions, and the composition of DIC in Neoproterozoic oceans. *Proceedings of the National Academy of Sciences*, *116*(38), 18874–18879. https://doi.org/10.1073/pnas.1909570116

Hofmann, H. J. (1981). First record of a Late Proterozoic faunal assemblage in the North American Cordillera. *Lethaia*, *14*(4), 303–310. https://doi.org/10.1111/j.1502-3931.1981.tb01103.x

Husson, J. M., Higgins, J. A., Maloof, A. C., & Schoene, B. (2015). Ca and Mg isotope constraints on the origin of Earth's deepest δ13C excursion. *Geochimica et Cosmochimica Acta*, *160*, 243–266. https://doi.org/10.1016/j.gca.2015.03.012

Husson, J. M., Linzmeier, B. J., Kitajima, K., Ishida, A., Maloof, A. C., Schoene, B., Peters, S. E., & Valley, J. W. (2020). Large isotopic variability at the micron-scale in 'Shuram' excursion carbonates from South Australia. *Earth and Planetary Science Letters*, *538*, 116211. https://doi.org/10.1016/j.epsl.2020.116211

Husson, J. M., Maloof, A. C., Schoene, B., Chen, C. Y., & Higgins, J. A. (2015). Stratigraphic expression of Earth's deepest 13C excursion in the Wonoka Formation of South Australia. *American Journal of Science*, *315*(1), 1–45. https://doi.org/10.2475/01.2015.01

James, N. P., & Wood, R. A. (2010). Reefs. In I. N. P. James & R. W. Dalrymple (Eds.), *Facies Models* (Vol. 4, pp. 421–447). Geological Association of Canada.

Jeletzky, J. A. (1962). Pre-Cretaceous Richardson Mountains Trough – its place in the tectonic framework of Arctic Canada and its bearing on some geosynclinals concepts. *Transactions of the Royal Society of Canada*, *56*, 55–84.

Jiang, G., Kennedy, M. J., & Christie-Blick, N. (2003). Stable isotopic evidence for methane seeps in Neoproterozoic postglacial cap carbonates. *Nature*, *426*(6968), 822–826. https://doi.org/10.1038/nature02201

Kaufman, A. J., Knoll, A. H., & Narbonne, G. M. (1997). Isotopes, ice ages, and terminal Proterozoic earth history. *Proceedings of the National Academy of Sciences*, *94*(13), 6600–6605. https://doi.org/10.1073/pnas.94.13.6600

Kendall, B., Creaser, R. A., & Selby, D. (2009). ^{187}Re-^{187}Os geochronology of Precambrian organic-rich sedimentary rocks. *Geological Society, London, Special Publications*, *326*(1), 85–107. https://doi.org/10.1144/sp326.5

Knauth, L. P., & Kennedy, M. J. (2009). The late Precambrian greening of the Earth. *Nature*, *460*(7256), 728–732. https://doi.org/10.1038/nature08213

Lamontagne, R. A., Swinnerton, J. W., Linnenbom, V. J., & Smith, W. D. (1973). Methane concentrations in various marine environments. *Journal of Geophysical Research*, *78*(24), 5317–5324. https://doi.org/10.1029/jc078i024p05317

Lazar, B., & Erez, J. (1992). Carbon geochemistry of marine-derived brines: I. 13C depletions due to intense photosynthesis. *Geochimica et Cosmochimica Acta*, *56*(1), 335–345. https://doi.org/10.1016/0016-7037(92)90137-8

Lemon, N. M. (2000). A Neoproterozoic fringing stromatolite reef complex, Flinders Ranges, South Australia. *Precambrian Research*, *100*(1–3), 109–120. https://doi.org/10.1016/s0301-9268(99)00071-6

Li, C., Hardisty, D. S., Luo, G., Huang, J., Algeo, T. J., Cheng, M., Shi, W., An, Z., Tong, J., Xie, S., Jiao, N., & Lyons, T. W. (2017). Uncovering the spatial heterogeneity of Ediacaran carbon cycling. *Geobiology*, *15*(2), 211–224. https://doi.org/10.1111/gbi.12222

Link, P. K., Todt, M. K., Pearson, D. M., & Thomas, R. C. (2017). 500–490 Ma detrital zircons in Upper Cambrian Worm Creek and correlative sandstones, Idaho, Montana, and Wyoming: Magmatism and tectonism within the passive margin. *Lithosphere*, *9*(6), 910–926. https://doi.org/10.1130/l671.1

Macdonald, F. A., Schmitz, M. D., Crowley, J. L., Roots, C. F., Jones, D. S., Maloof, A. C., Strauss, J. V., Cohen, P. A., Johnston, D. T., & Schrag, D. P. (2010). Calibrating the Cryogenian. *Science*, *327*(5970), 1241–1243. https://doi.org/10.1126/science.1183325

Macdonald, F. A., Schmitz, M. D., Strauss, J. V., Halverson, G. P., Gibson, T. M., Eyster, A., Cox, G., Mamrol, P., & Crowley, J. L. (2018). Cryogenian of Yukon. *Precambrian Research*, *319*, 114–143. https://doi.org/10.1016/j.precamres.2017.08.015

Macdonald, F. A., Strauss, J. V., Sperling, E. A., Halverson, G. P., Narbonne, G. M., Johnston, D. T., Kunzmann, M., Schrag, D. P., & Higgins, J. A. (2013). The stratigraphic relationship between the Shuram carbon isotope excursion, the oxygenation of Neoproterozoic oceans, and the first appearance of the Ediacara biota and bilaterian trace fossils in northwestern Canada. *Chemical Geology*, *362*, 250–272. https://doi.org/10.1016/j.chemgeo.2013.05.032

MacNaughton, R. B., Narbonne, G. M., & Dalrymple, R. W. (2000). Neoproterozoic slope deposits, Mackenzie Mountains, northwestern Canada: implications for passive-margin development and Ediacaran faunal ecology. *Canadian Journal of Earth Sciences*, *37*(7), 997–1020. https://doi.org/10.1139/e00-012

MacNaughton, R. B., Roots, C. F., & Martel, E. (2008). *Neoproterozoic-(?)Cambrian lithostratigraphy, northeast Sekwi Mountain map area, Mackenzie Mountains, Northwest Territories: new data from measured sections* (Current Research No. 2008–16). Geological Survey of Canada. https://doi.org/10.4095/225901

Maslyn, R. M. (1977). *Recognition of fossil karst features in the ancient record: A discussion of several common fossil karst forms. Exploration Frontiers of the Central and Southern Rockies*. Rocky Mountain Association of Geologists.

Matthews, J. J., Liu, A. G., Yang, C., McIlroy, D., Levell, B., & Condon, D. J. (2021). A chronostratigraphic framework for the rise of the Ediacaran macrobiota: New constraints from Mistaken Point Ecological Reserve, Newfoundland. *GSA Bulletin*, *133*(3–4), 612–624. https://doi.org/10.1130/b35646.1

Medig, K. P. R., Turner, E. C., Thorkelson, D. J., & Rainbird, R. H. (2016). Rifting of Columbia to form a deep-water siliciclastic to carbonate succession: The Mesoproterozoic Pinguicula Group of northern Yukon, Canada. *Precambrian Research*, *278*, 179–206. https://doi.org/10.1016/j.precamres.2016.03.021

Merino, E., & Banerjee, A. (2008). Terra rossa genesis, implications for karst and eolian dust: A geodynamic thread. *The Journal of Geology*, *116*(1), 62–75. https://doi.org/10.1086/524675

Morrow, D. W. (1999). *Lower Paleozoic stratigraphy of northern Yukon Territory and northwestern District of Mackenzie*. Geological Survey of Canada. https://doi.org/10.4095/210998

Moscardelli, L., & Wood, L. (2008). New classification system for mass transport complexes in offshore Trinidad. *Basin Research*, *20*(1), 73–98. https://doi.org/10.1111/j.1365-2117.2007.00340.x

Moynihan, D. P. (2014). Bedrock Geology of NTS 106B/04, Eastern Rackla belt. In K. E. MacFarlane, M. G. Nordling, P. J. Sack, & P. J (Eds.), *Yukon Exploration and Geology 2013* (pp. 147–167).

Moynihan, D. P. (2016). *Bedrock geology compilation of the eastern Rackla belt, NTS 105N/15, 105N/16, 105O/13, 106B/4, 106C/1, 106C/2, east-central Yukon* [Open-File Report]. Yukon Geological Survey.

Moynihan, D. P., Strauss, J. V., Nelson, L. L., & Padget, C. D. (2019). Upper Windermere Supergroup and the transition from rifting to continent-margin sedimentation, Nadaleen River area, northern Canadian Cordillera. *GSA Bulletin*, *131*(9–10), 1673–1701. https://doi.org/10.1130/b32039.1

Mustard, P. S. (1991). Normal faulting and alluvial-fan deposition, basal Windermere Tectonic Assemblage, Yukon, Canada. *GSA Bulletin*, *103*(10), 1346–1364. https://doi.org/10.1130/0016-7606(1991)103

Mustard, P. S., & Roots, C. J. F. (1997). *Rift-related volcanism, sedimentation, and tectonic setting of the Mount Harper Group, Ogilvie Mountains, Yukon Territory*. Geological Survey of Canada. https://doi.org/10.4095/208670

Myrow, P. M., Tice, L., Archuleta, B., Clark, B., Taylor, J. F., & Ripperdan, R. L. (2004). Flat-pebble conglomerate: its multiple origins and relationship to metre-scale depositional cycles. *Sedimentology*, *51*(5), 973–996. https://doi.org/10.1111/j.1365-3091.2004.00657.x

Narbonne, G. M. (1994). New Ediacaran fossils from the Mackenzie Mountains, northwestern Canada. *Journal of Paleontology*, *68*(3), 411–416. https://doi.org/10.1017/s0022336000025816

Narbonne, G. M., & Aitken, J. (1995). Neoproterozoic of the Mackenzie Mountains, northwestern Canada. *Precambrian Research*, *73*(1–4), 101–121. https://doi.org/10.1016/0301-9268(94)00073-z

Narbonne, G. M., & Aitken, J. D. (1990). Ediacaran fossils from the Sekwi Brook area, Mackenzie Mountains, northwestern Canada. *Palaeontology*, *33*(4), 945–980.

Narbonne, G. M., Hofmann, H. J., & Aitken, J. D. (1985). *Precambrian-cambrian boundary sequence, Wernecke Mountains, Yukon Territory* (Current Research Part A Paper 85-1A; pp. 603–608). Geological Survey of Canada. https://doi.org/10.4095/120164

Narbonne, G. M., Kaufman, A. J., & Knoll, A. H. (1994). Integrated chemostratigraphy and biostratigraphy of the Windermere Supergroup, northwestern Canada: Implications for Neoproterozoic correlations and the early evolution of animals. *GSA Bulletin*, *106*(10), 1281–1292. https://doi.org/10.1130/0016-7606(1994)106

Narbonne, G. M., Laflamme, M., Trusler, P. W., Dalrymple, R. W., & Greentree, C. (2014). Deep-water Ediacaran fossils from northwestern Canada: Taphonomy, ecology, and evolution. *Journal of Paleontology*, *88*(2), 207–223. https://doi.org/10.1666/13-053

Norris, D. K. (1982). *Geology: Snake River, Yukon Territory-Northwest Territories (District of Mackenzie). Map 1529A*. Geological Survey of Canada.

Okulitch, A. V., & Irwin, D. (2016). *Geological Compilation of the Western Mainland and Arctic Islands of the Northwest Territories* [NWT Open File Report 2016-09.]. Northwest Territories Geoscience Office.

Osborne, D. T., Narbonne, G. M., & Carrick, J. (1986). Stratigraphy and economic potential of Precambrian - Cambrian boundary strata, Wernecke Mountains, east-central Yukon. *Yukon Geology*, *1*, 131–138.

Pinet, N., Davis, W. J., Petts, D. C., Sack, P., Mercier-Langevin, P., Lavoie, D., & Jackson, S. E. (2022). U-Pb vein calcite dating reveals the age of Carlin-type gold deposits of central Yukon and a contemporaneity with a regional intrusion-related metallogenic event. *Economic Geology*, *117*(4), 905–922. https://doi.org/10.5382/econgeo.4898

Playton, T. E., Janson, X., Kerans, C., James, N. P., & Dalrymple, R. W. (2010). Carbonate Slopes. In N. P. James & R. W. Dalrymple (Eds.), *Facies Models* (Vol. 4, pp. 449–476). Geological Association of Canada.

Post, R. T., & Long, D. G. F. (2008). The Middle Cambrian Mount Roosevelt Formation (new) of northeastern British Columbia: evidence for rifting and development of the Kechika Graben System. *Canadian Journal of Earth Sciences*, *45*(4), 483–498. https://doi.org/10.1139/e08-014

Prather, M. (1995). Other trace gases and atmospheric chemistry. *Climate Change*, 77–126.

Pyle, L. J., Narbonne, G. M., James, N. P., Dalrymple, R. W., & Kaufman, A. J. (2004). Integrated Ediacaran chronostratigraphy, Wernecke Mountains, northwestern Canada. *Precambrian Research*, *132*(1–2), 1–27. https://doi.org/10.1016/j.precamres.2004.01.004

Rankey, E. C., & Reeder, S. L. (2011). Holocene oolitic marine sand complexes of the Bahamas. *Journal of Sedimentary Research*, *81*(2), 97–117. https://doi.org/10.2110/jsr.2011.10

Read, J. F. (1985). Carbonate platform facies models. *AAPG Bulletin*, *69*(1), 1–21. https://doi.org/10.1306/ad461b79-16f7-11d7-8645000102c1865d

Read, J. F., & Grover, G. A. (1977). Scalloped and planar erosion surfaces, Middle Ordovician limestones, Virginia; analogues of Holocene exposed karst or tidal rock platforms. *Journal of Sedimentary Research*, *47*(3), 956–972. https://doi.org/10.1306/212f72bb-2b24-11d7-8648000102c1865d

Rooney, A. D., Cantine, M. D., Bergmann, K. D., Gómez-Pérez, I., Al Baloushi, B., Boag, T. H., Busch, J. F., Sperling, E. A., & Strauss, J. V. (2020). Calibrating the coevolution of Ediacaran life and environment. *Proceedings of the National Academy of Sciences*, *117*(29), 16824–16830. https://doi.org/10.1073/pnas.2002918117

Rooney, A. D., Strauss, J. V., Brandon, A. D., & Macdonald, F. A. (2015). A Cryogenian chronology: Two long-lasting synchronous Neoproterozoic glaciations. *Geology*, *43*(5), 459–462. https://doi.org/10.1130/g36511.1

Roots, C. F., Abbott, J. G., Cecile, M. P., & Gordey, S. P. (1995). *Bedrock geology of Lansing map area (105N) east half, Hess Mountains, Yukon. Open File 1995-7*. Indian and Northern Affairs Canada, Exploration and Geological Services Division. https://doi.org/10.4095/205738

Rose, C. V., Swanson-Hysell, N. L., Husson, J. M., Poppick, L. N., Cottle, J. M., Schoene, B., & Maloof, A. C. (2012). Constraints on the origin and relative timing of the Trezona δ13C anomaly below the end-Cryogenian glaciation. *Earth and Planetary Science Letters*, *319–320*, 241–250. https://doi.org/10.1016/j.epsl.2011.12.027

Ross, G. M. (1991). Tectonic setting of the Windermere Supergroup revisited. *Geology*, *19*(11), 1125–1128. https://doi.org/10.1130/0091-7613(1991)019

Ross, G. M., Bloch, J., & Krouse, H. (1995). Neoproterozoic strata of the southern Canadian Cordillera and the isotopic evolution of seawater sulfate. *Precambrian Research*, *73*(1–4), 71–99. https://doi.org/10.1016/0301-9268(94)00072-y

Rothman, D. H., Hayes, J. M., & Summons, R. E. (2003). Dynamics of the Neoproterozoic carbon cycle. *Proceedings of the National Academy of Sciences*, *100*(14), 8124–8129. https://doi.org/10.1073/pnas.0832439100

Sarmiento, J. L., & Gruber, N. (2006). *Ocean Biogeochemical Dynamics*. Princeton University Press. https://doi.org/10.1515/9781400849079

Schiffbauer, J. D., Huntley, J. W., O'Neil, G. R., Darroch, S. A. F., Laflamme, M., & Cai, Y. (2016). The latest Ediacaran Wormworld fauna: Setting the ecological stage for the Cambrian Explosion. *GSA Today*, *26*(11), 4–11. https://doi.org/10.1130/gsatg265a.1

Schrag, D. P., Higgins, J. A., Macdonald, F. A., & Johnston, D. T. (2013). Authigenic carbonate and the history of the global carbon cycle. *Science*, *339*(6119), 540–543. https://doi.org/10.1126/science.1229578

Soto-Kerans, P., Loucks, R. G., & Kerans, C. (2021). Deeper-water deposition in intrashelf basins: Example from the Lower Cretaceous (Albian) upper Glen Rose Formation in the Houston trough, eastern Texas. *AAPG Bulletin*, *105*(7), 1405–1434. https://doi.org/10.1306/12222019055

Sperling, E. A., Carbone, C. A., Strauss, J. V., Johnston, D. T., Narbonne, G. M., & Macdonald, F. A. (2015). Oxygen, facies, and secular controls on the appearance of Cryogenian and Ediacaran body and trace fossils in the Mackenzie Mountains of northwestern Canada. *Geological Society of America Bulletin*, *128*(3–4), 558–575. https://doi.org/10.1130/b31329.1

Strauss, J. V., MacDonald, F. A., Halverson, G. P., Tosca, N. J., Schrag, D. P., & Knoll, A. H. (2015). Stratigraphic evolution of the Neoproterozoic Callison Lake Formation: Linking the break-up of Rodinia to the Islay carbon isotope excursion. *American Journal of Science*, *315*(10), 881–944. https://doi.org/10.2475/10.2015.01

Strauss, J. V., Rooney, A. D., Macdonald, F. A., Brandon, A. D., & Knoll, A. H. (2014). 740 Ma vase-shaped microfossils from Yukon, Canada: Implications for Neoproterozoic chronology and biostratigraphy. *Geology*, *42*(8), 659–662. https://doi.org/10.1130/g35736.1

Thorkelson, D. J., Abbott, J. G., Mortensen, J. K., Creaser, R. A., Villeneuve, M. E., McNicoll, V. J., & Layer, P. W. (2005). Early and middle Proterozoic evolution of Yukon, Canada. *Canadian Journal of Earth Sciences*, *42*(6), 1045–1071. https://doi.org/10.1139/e04-075

Thorkelson, D. J., & Wallace, C. A. (1998). *Geological map of Dolores Creek area, Wernecke Mountains, Yukon (106C/14)*. Indian & Northern Affairs Canada/ Department of Indian & Northern Development: Exploration & Geological Services Division.

Trower, E. J., Cantine, M. D., Gomes, M. L., Grotzinger, J. P., Knoll, A. H., Lamb, M. P., Lingappa, U., O'Reilly, S. S., Present, T. M., Stein, N., Strauss, J. V., & Fischer, W. W. (2018). Active ooid growth driven by sediment transport in a high-energy shoal, Little Ambergris Cay, Turks and Caicos Islands. *Journal of Sedimentary Research*, *88*(9), 1132–1151. https://doi.org/10.2110/jsr.2018.59

Tucker, M. J., Hart, C. J. R., & Carne, R. C. (2012). Geology, alteration, and mineralization of the Carlin-type Conrad zone, Yukon. *Yukon Exploration and Geology*, 163–178.

United States Geological Survey. (2019). *3D Elevation Program 1-Meter Resolution Digital Elevation Model*. https://www.usgs.gov/the-national-map-data-delivery

Yang, C., Rooney, A. D., Condon, D. J., Li, X.-H., Grazhdankin, D. V., Bowyer, F. T., Hu, C., Macdonald, F. A., & Zhu, M. (2021). The tempo of Ediacaran evolution. *Science Advances*, *7*(45), 9643. https://doi.org/10.1126/sciadv.abi9643

Young, G. M., Jefferson, C. W., Delaney, G. D., & Yeo, G. M. (1979). Middle and late Proterozoic evolution of the northern Canadian Cordillera and Shield. *Geology*, *7*(3), 125–128. https://doi.org/10.1130/0091-7613(1979)7

Yukon Geological Survey. (2022). *Yukon Digital Bedrock Geology*. https://data.geology.gov.yk.ca/Compilation/3

Zeebe, R. E., & Westbroek, P. (2003). A simple model for the $CaCO_3$saturation state of the ocean: The "Strangelove," the "Neritan," and the "Cretan" Ocean. *Geochemistry, Geophysics, Geosystems*, *4*(12). https://doi.org/10.1029/2003gc000538

Supplementary Materials

Busch et al supplementary information

Download: https://ajsonline.org/article/74874-integrated-litho-chemo-nbsp-and-sequence-stratigraphy-of-the-ediacaran-gametrail-formation-across-a-shelf-slope-transect-in-the-wernecke-mountains/attachment/158047.zip